Fendley Isabel, M. (Orcid ID: 0000-0001-8142-6799)

Arz Jose, A. (Orcid ID: 0000-0003-0063-8752)

Gilabert Vicente (Orcid ID: 0000-0001-7302-5901)

Vanderkluysen Loÿc (Orcid ID: 0000-0001-8263-1604)

Smit Jan (Orcid ID: 0000-0002-6070-4865)

Mittal Tushar (Orcid ID: 0000-0002-8026-0018)

No Cretaceous-Paleogene Boundary in Exposed Rajahmundry Traps: A Refined Chronology of the Longest Deccan Lava Flows From ^{40}Ar/^{39}Ar Dates, Magnetostratigraphy, and Biostratigraphy

Isabel M. Fendley[1], Courtney J. Sprain[2], Paul R. Renne[1,3], Ignacio Arenillas[4], José A. Arz[4], Vicente Gilabert[4], Stephen Self[1], Loÿc Vanderkluysen[5], Kanchan Pande[6], Jan Smit[7], Tushar Mittal[1]*

[1]University of California Berkeley, Department of Earth and Planetary Science, 307 McCone Hall, Berkeley, CA, 94720, United States

[2]University of Florida, Department of Geological Sciences, 241 Williamson Hall, Gainesville, FL, 32611, United States

[3]Berkeley Geochronology Center, 2455 Ridge Rd Berkeley, CA, 94709, United States

[4]Universidad Zaragoza, Departamento de Ciencias de la Tierra and Instituto Universitario de Investigación en Ciencias Ambientales de Aragón. Pedro Cerbuna 12, 50009 Zaragoza, Spain

[5]Drexel University, Department of Biodiversity, Earth and Environmental Science, 2024 MacAlister Hall, 3250 Chestnut Street, Philadelphia, PA, 19104, United States

[6]Indian Institute of Technology Bombay, Department of Earth Sciences, Powai, Mumbai 400076, India

[7]Vrije Universiteit Amsterdam, Department of Geology and Geochemistry, Faculty of Science, 1081 HV Amsterdam, The Netherlands

*Current address: Massachusetts Institute of Technology, Department of Earth, Atmosphere, and Planetary Sciences, 77 Massachusetts Avenue, Cambridge, MA, 02139, United States

Corresponding author: Isabel Fendley (isabel.fendley@berkeley.edu)

Key Points:

- Exposed Rajahmundry Traps lava flows were all erupted after the Cretaceous-Paleogene boundary, between 65.92 and 65.27 million years ago

- Rajahmundry Traps consistent with Deccan Traps chrono- and chemostratigraphy, thus are very long flows from main Deccan eruptive vents

- Model and climate records show that eruptive CO_2 release from large individual Deccan eruptions is insufficient to cause significant warming

Abstract

Deccan Traps flood basalt volcanism affected ecosystems spanning the end-Cretaceous mass extinction, with the most significant environmental effects hypothesized to be a consequence of the largest eruptions. The Rajahmundry Traps are the farthest exposures (~1000 km) of Deccan basalt from the putative eruptive centers in the Western Ghats, and hence represent some of the largest volume Deccan eruptions. Although the three subaerial Rajahmundry lava flows have been geochemically correlated to the Wai Subgroup of the Deccan Traps, poor precision associated with previous radioisotopic age constraints has prevented detailed comparison with potential climate effects. In this study, we use new $^{40}Ar/^{39}Ar$ dates, paleomagnetic and volcanological analyses, and biostratigraphic constraints for the Rajahmundry lava flows to ascertain the timing and style of their emplacement. We find that the lower and middle flows (65.92±0.25 and 65.67±0.08 Ma, ±1σ systematic

uncertainty) were erupted within magnetochron C29r and were a part of the Ambenali Formation of the Deccan Traps. By contrast, the uppermost flow (65.27±0.08 Ma) was erupted in C29n as part of the Mahabaleshwar Formation. Given these age constraints, the Rajahmundry flows were not involved in the end-Cretaceous extinction as previously hypothesized. To determine whether the emplacement of the Rajahmundry flows could have affected global climate, we estimated their eruptive CO_2 release and corresponding climate change using scalings from the LOSCAR carbon cycle model. We find that the eruptive gas emissions of these flows were insufficient to directly cause multi-degree warming, hence a causal relationship with significant climate warming requires additional Earth system feedbacks.

Plain Language Summary

Flood basalt eruptions are among the largest volcanic eruptions in Earth's history and are frequently associated with mass extinctions. The Deccan Traps flood basalt erupted close in time to the end-Cretaceous mass extinction, which marked the demise of the dinosaurs. We determine the timing of the largest known Deccan eruptions, the Rajahmundry Traps, which are potentially the longest lava flows in the world. These eruptions were thought to have played a role in the mass extinction. We estimate when these eruptions happened using techniques including $^{40}Ar/^{39}Ar$ radioisotopic dating, paleomagnetism, micropaleontology, and geochemistry. We find that the Rajahmundry Traps erupted after the mass extinction. Additionally, we find that the eruptions happened around the same time interval as climate warming which may have impacted the ecological recovery after the mass extinction. We model the climate effects of the Rajahmundry eruptions and find that their eruptive CO_2 emissions were likely not enough to directly cause multi-degree warming. However, volcanic systems may non-eruptively emit CO_2 or may cause other environmental effects which could indirectly increase the amount of climate warming.

1. Introduction

The Deccan Traps continental flood basalt eruptions spanned the Cretaceous-Paleogene boundary mass extinction event, with >90% of the volume emplaced in approximately 1 million years (e.g., Courtillot et al., 1986; Schoene et al., 2019; Sprain et al., 2019). It is estimated that at least 1 million km^3 of basalt was erupted, forming the Main Deccan Volcanic Province (MDVP, Fig. 1a), best exposed in the Western Ghats, along with several other smaller provinces including the Mandla Lobe and Malwa Plateau (e.g., Mahoney, 1988; Raja Rao et al., 1978). The periods of largest eruptive flux are hypothesized to correspond to the most significant climate effects, via eruptive CO_2 and SO_2 release (e.g., Self et al., 2006). Understanding of eruptive timing and flux is required to estimate eruptive CO_2 emissions and hence directly compare eruptive history, hypothesized climate effects, and climate records. Consequently, constraining the timing and volume of the largest eruptions is one crucial part of understanding and testing the mechanisms through which Deccan eruptions impacted the environment. In particular, these constraints can help us assess the importance of eruptive versus non-eruptive degassing of magmatic volatiles for Deccan-associated climate change (e.g., Hull et al., 2020; Sprain et al., 2019).

The exposed Rajahmundry Traps (RT) in eastern India potentially represent some of the largest volume Deccan Traps eruptions as they are ~1000 km from the hypothesized Deccan eruptive centers near the present-day east coast of India, and ~400 km from any other exposures of Deccan basalt (Fig. 1) (e.g., Baksi, 2001; Baksi et al., 1994; Self et al., 2008; Vanderkluysen et al., 2011). Each Rajahmundry flow therefore corresponds with an erupted volume of ~1000-6000 km^3 (length of 1000 km, width of 50-200 km and thickness of 20-30 m). This is comparable to the largest flow fields of the Siberian Traps flood basalts and the Columbia River Basalts (Krivolutskaya & Kedrovskaya, 2020; Vye-Brown et al., 2013).

Despite the great distance between them, the RT outcrops have long been associated with the Deccan Traps due to their geochemical and temporal similarity (Baksi et al., 1994; Blandford, 1867; Jay and Widdowson, 2008; Keller et al., 2008; Knight et al., 2003). Some previous work suggested that the RT basalts span the Cretaceous-Paleogene boundary and the C29r/C29n magnetic reversal. Previous $^{40}Ar/^{39}Ar$ dates indicated the RT are late Cretaceous to early Paleocene in age (~63−67 Ma) (Knight et al., 2003), and paleomagnetic analyses found that flows with normal magnetic polarity overlie reversely magnetized flows (Baksi, 2001; Vandamme and Courtillot, 1992). Additionally, Danian fossils found in a carbonate sequence between the lower two flows (e.g., Baksi et al., 1994; Keller et al., 2008; Sen and Sabale, 2011), and Maastrichtian fossils in the sediments below the lowest flow (e.g., Keller et al., 2008; Mukherjee et al., 2013) suggested that the lowest flow was emplaced in the latest Cretaceous. These chronologic constraints led to the hypothesis that the lowest flow is part of an extremely voluminous Deccan eruptive episode just prior to the mass extinction and Cretaceous-Paleogene boundary (e.g., Keller et al., 2008, 2012; Lakshminarayana et al., 2010).

However, there has been no high-resolution and consistent chronostratigraphic framework for the region. One of the primary reasons for this is that exposures in the Rajahmundry area are only in active quarries - meaning that sampling locations, plus which lava flows are exposed, and even quarry names, are constantly changing over time. Consequently, it is challenging to assemble literature data, collected over decades, into a consistent chronostratigraphic framework. For instance, earlier studies describe the RT as having either two or three exposed flows depending on the sampling locality (e.g., Baksi et al., 1994; Keller et al., 2008; Sen and Sabale, 2011). Thus, for example, the precise stratigraphic location of the reverse to normal polarity transition is unclear due to these sampling uncertainties (Baksi, 2001; Knight et al., 2003; Subbarao and Pathak, 1993).

To ascertain potential climate or ecological impacts of the RT and Deccan eruptions more broadly, there is a need to determine a more precise timing of these large eruptions. In one commonly used stratigraphic scheme, the Deccan Traps basalts are divided into formations based on their chemistry, and these formations are assumed to be isochronous throughout the Main Deccan Volcanic Province (Beane et al., 1986). Determining the timing of the RT eruptions is necessary in order to evaluate whether the RT are compatible with the contemporaneous MDVP geochemical formations. The RT have previously been shown to be most geochemically similar to the Ambenali and Mahabaleshwar Formations (Baksi, 2001). However, the previous dates on the RT failed to demonstrate more than broad agreement with this assignment, since with an age uncertainty of ~0.5 -1 Ma, the RT flows coincide with a large fraction of the main Deccan Traps eruptive period (Knight et al., 2003). With a refined chronostratigraphic framework for the RT, we can test whether the RT flows are still consistent with new high-resolution age constraints for these formations from the Western Ghats (Schoene et al., 2019; Sprain et al., 2019).

In this study, new geochronology for the RT refines their relationship with up to date geochemical stratigraphy and geochronology from the Western Ghats. This new chronostratigraphic framework refines the timing and eruptive rate of the RT eruptions, particularly with respect to the Cretaceous-Paleogene boundary. The updated framework allows us to assess the potential of the RT flows to have perturbed climate during the mass extinction and recovery.

2. Methods and Data

2.1 Geologic setting: volcanology and site descriptions

The RT consist of a set of lava flows that have sediment beds between them (termed intertrappean sediments) and just below them (infratrappean sediments). This package is

bounded by unconformities: the uppermost lava flow is directly overlain by the Eocene Rajahmundry sandstone, and the approximately conformable infratrappean sediments are underlain by the early to mid-Cretaceous Tirupati Formation (e.g. Bhalla, 1966; Geological Survey of India, 2000a; 2000b). Three lava flows and the overlying Rajahmundry sandstone are exposed in two quarries on the western side of the Godavari River, leaving no uncertainty with respect to their relative stratigraphy (Fig. 1b, Fig. 2a). Only one flow is exposed on the eastern side of the Godavari, which we and others parsimoniously interpret to be the uppermost flow from the western side, as it is overlain directly by an erosive contact with the Rajahmundry sandstone (Baksi, 2001; Fig. 2b). This assignment is corroborated by our geochronology and magnetostratigraphy (Sections 2.2 and 2.3). The lowermost exposed flow is underlain by a highly fossiliferous marine marl to sandstone infratrappean unit which is potentially Maastrichtian in age (Fig. S1a) (e.g., Sen and Sabale, 2011). While only three flows are exposed at the surface, several more, of unknown age, are documented in sub-surface drill cores (Keller et al., 2011), and there is no exposed contact between the infratrappean sediments (or lowest exposed lava flow) and the underlying Tirupati Formation (Bhalla, 1966).

We logged five quarry exposures, four on the western side of the Godavari River and one on the eastern side, all of which display fresh material and near vertical sections. After accounting for the relative location of the quarries, and factoring in the slight regional tilt to the south/south east towards the coast (e.g., Sahu et al., 2013), we conclude that the exposed Rajahmundry Traps comprise three lava flows, formed by three separate eruptions, consistent with some previous work (e.g., Lakshminarayana et al., 2010; Sen and Sabale, 2011). Reports of different numbers of lava flows in previous studies were most likely due to limited exposure caused by regional tilt and the presence of water tables at the base of flows. We

here designate the lower, middle, and upper of the three flows as Flows 1, 2, and 3, respectively.

The lowest and thickest of the three lava flows (Flow 1) is approximately 30 m thick. Its base shows evidence for water-rock interaction such as rootless cones and entablature exhibiting fine columnar and radial jointing (Fig. S2a-b). It is a compound flow, with at least three or four thick inflated sheet lobes which display entablature, and the top of the flow forms a colonnade (Fig. S3a-b).

Flow 1 is separated from the Flow 2 by a sedimentary intertrappean bed which was deposited in a near coastal marine setting (e.g., Mallick et al., 2014, Fig. S1b-c). The middle of this unit is generally highly fossiliferous limestone to marl, with more clay and silt towards the top. In one exposure (Government Quarry) there is a charcoal layer at the top, suggesting that Flow 2 erupted onto a layer of terrestrial vegetation (Fig. S1d). The thickness of the entire unit is between 3 and 5 m depending on location, and the lower part generally shows evidence of recrystallization and hydrothermal alteration (Keller et al., 2008).

Flow 2 and Flow 3 are both ~20 m thick and have columnar jointing throughout. They generally possess no fluid-lava interaction features, indicating they were emplaced onto land or into extremely shallow water (Fig. S4a-b). However, in Gowripatnam Quarry Flow 2 has a second thin (1-2 m) lobe at the base with a finely jointed and highly vesicular texture, indicating rapid cooling (Fig. S5a-b). Flows 2 and 3 are separated by a 1-2 m thick sediment layer which is formed of red clay and is extremely similar in appearance to a very thick "red bole" of the main Deccan province (e.g., Ghosh et al., 2006; Sen and Sabale, 2011; Widdowson et al., 1997) (Fig. S6). There are no fossils of any kind, suggesting negligible marine influence.

Our observations are in agreement with the previous conclusion that the first lava flow was emplaced into shallow water, corroborated by the shallow marine infratrappean and carbonate intertrappean units, whereas the upper two flows and the red bole were emplaced subaerially (e.g. Keller et al., 2008; Self et al., 2008; Sen and Sabale, 2011). We interpret the Knight et al. (2003), Self et al. (2008), and Keller et al. (2008) "upper flow" to be equivalent to our Flow 2 on the western side of the river, as there is limited exposure of the Flow 3 in those quarries, and Flow 1 is easily distinguished from Flow 2 because of the highly visible carbonate intertrappean unit at the top of Flow 1. On the eastern side of the river we have assigned the "upper flow" to Flow 3, as it is the only flow exposed in that area and it is overlain by the Rajahmundry sandstone.

2.2 Paleomagnetic analysis

Samples for paleomagnetic analysis were selected from seven horizons, two from Flow 1, three from Flow 2, and two from Flow 3, collected from the Gowripatnam, Government, Church, and Rajahmundry Quarries (Fig. 1b, Fig. S7a). At least three oriented blocks were collected from each horizon. One to three oriented 10-cm^3 specimen cubes were cut out of each block sample using a wet tile saw. After cutting, samples were sanded and blown with pressurized air to remove extraneous material from saw blades. All three lava flows had dips of only a few degrees, due to the regional tilt of $\leq 5°$ to the south-southeast (Baksi, 2001). Tilt corrections were not performed, as they would alter the absolute direction by only a few degrees and all flows were similarly oriented.

Flow 1: Two horizons (RJ17-1 and RJ17-2, Fig. S7a) from Flow 1 were sampled from the Gowripatnam Quarry. RJ17-1 was collected from the bottom of Flow 1, within 3-5 meters of the base of the flow and ~25 m from the intertrappean. Here, the lava flow displays closely spaced columnar jointing/entablature. RJ17-2 was collected from the top of Flow 1,

roughly 5 m below the intertrappean. Samples were collected within the upper colonnade/top of the entablature.

Flow 2: Three horizons were sampled from Flow 2. One horizon from the base of the flow (RJ17-3), ~ 2 m above the intertrappean, was collected from the Gowripatnam Quarry. The other two were collected from the Government Quarry (RJ17-6 and RJ17-7). RJ17-7 was collected from the lower columnar jointed portion of Flow 2, ~ 4-5 m above the top of the intertrappean. RJ17-6 was collected from the middle part of Flow 2, ~ 7-10 m below the red bole topping Flow 2. Samples were collected at the top of coarsely spaced columnar joints (~ 1 m spacing), close to the top of the core of the flow.

Flow 3: One horizon (RJ17-5) from Flow 3 was collected at the Church Quarry from the basal portion of the flow, ~ 2 m above the red bole horizon. The samples were collected from the basal columnar jointed region of the flow. There is abundant spheroidal weathering on exposed surfaces, but samples look unaltered when broken open. Across the Godavari River, one horizon (RJ17-4) was collected from Flow 3 within the Rajahmundry Quarry. RJ17-4 was collected ~ 1 m from the base of the Quarry within the lower part of the core of the flow, ~ 20 m below the contact with the Rajahmundry Formation sandstone.

We performed demagnetization experiments at the Berkeley Geochronology Center (BGC). At least six specimens per horizon were demagnetized. We used a combination of stepwise alternating field (AF) and thermal demagnetization techniques. For stepwise demagnetization, samples underwent alternating field demagnetization using an in-line 2-axis static degausser associated with the 2G-755R cryogenic magnetometer, starting at fields ~ 3 mT and going up to fields of 100 mT, in 3-10 mT steps. Following AF demagnetization, samples underwent two thermal demagnetization steps at temperatures of 80ºC and 130ºC, to confirm that samples were not biased by a remanence held by goethite. Samples were heated

in a non-inductively wound ASC 48 specimen resistance furnace, housed within a magnetically shielded room at the BGC. In addition to stepwise AF demagnetization, we subjected at least one sample per horizon to a stepwise thermal demagnetization protocol. Before heating, samples were treated with low AF fields in steps of ~3 mT from 0-16 mT to remove viscous overprints. Samples were subsequently heated in 13 thermal steps starting at 100°C and ending at 580°C, with step sizes ranging from 100°C to 10°C near the magnetite Curie temperature. Susceptibility was measured after every thermal step to check for alteration. All samples were measured using the 2G-755R cryogenic magnetometer.

We determined the characteristic remanent magnetization (ChRM) directions of samples using linear trends toward the origin on Zijderveld plots using principal component analysis (Kirschvink, 1980) (Fig. S7b). We selected best-fit lines from a minimum of three consecutive demagnetization steps, where the maximum angle of deviation (MAD) was < 20 degrees (most MAD values were <10). Best-fit lines were not anchored to the origin so as to not bias directions by unremoved overprints. For one horizon, RJ17-6, we additionally determined ChRM directions using great circle analysis as the demagnetization data lay in a plane between the characteristic remanence and a secondary overprint (Fig. S7c). We performed data analysis using Demag GUI within the PmagPy software package (Tauxe et al., 2016).

We calculated flow means using Fisher statistics (Fisher, 1953). Only samples with directions determined via principal component analysis were used for flow mean calculations. To determine flow means, mean directions were determined at the sample level for each block (taking the Fisher mean of specimen-level results), and these block sample means were combined to determine flow mean directions. All flows passed Watson's test for randomness at the 95% confidence level (Watson, 1956).

In total, we determined ChRM directions for 55 specimens from three flows (See Fig. S7b for characteristic demagnetization diagrams and Table S2 for specimen-level results). Secondary overprints were commonly removed in low AF demagnetization steps (between 3-16 mT) and in thermal steps below 200°C. Secondary directions fall into three groups. A majority of secondary overprints are similar in direction to the present local field and most likely represent a recent viscous overprint. Within site RJ17-6, we observed an additional secondary overprint consistent in direction with the overlying flow direction (Fig. S7c). This component is held by a phase that has low unblocking temperature (<400°C), but higher coercivity that the ChRM and may be held by a titanomaghemite phase. It is most clearly removed during thermal demagnetization. Lastly, some samples have spurious random secondary overprints that were likely obtained due to blasting in the quarry, or stray fields during shipping. Characteristic directions were often constrained by 20 mT, or by 200°C. A majority of samples altered during heating and resulted in spurious directions in high-T steps but this did not impede the determination of ChRM directions. This alteration is associated with an increase in susceptibility starting ~300°C and is most likely associated with low-T oxidation and the presence of titanomaghemite. All specimens were completely demagnetized by 100 mT and 580°C, and do not show evidence of a high-coercivity, high-unblocking phase.

Based on the polarity and geochronologic results (Section 2.3), we assign Flows 1 and 2 to C29r and Flow 3 to C29n (Fig. 3b, Table 2). Looking at each flow's mean directions, Flow 1 has reverse polarity with a Dec = 158.7° and Inc = 78.6°. Flow 2 also has reverse polarity with Dec = 162.5° and Inc = 39.1°. Although Flow 1 and Flow 2 both have reverse polarity, their directions do not overlap within 95% confidence intervals, suggesting that some time passed between the eruption of these flows, consistent with the observed deposition of the intertrappean. Flow 2 is more closely associated with the expected direction

at that time with Dec = 163.5° and Inc = 49.7° (calculated using the apwp.py function of

PmagPy, which is based on the plate reconstruction model from Besse and Courtillot (2002)).

Flow 1 is much further from the expected direction and could be interpreted as a transitional

field. However, based on its age and the fact that lava flows record a snapshot of the field and

not a time-average, it is more likely that Flow 1 is recording a period of spurious secular

variation during a stable chron. Flow 3 has normal polarity with Dec = 301.1° and Inc = -

43.5°. This direction is similar but does not quite overlap with the expected direction at the

time of emplacement of Dec = 343.5° and Inc = -49.8°. Again, this discrepancy is likely due

to secular variation. Both samples from Flow 3 (from the Church and Rajahmundry Quarries)

overlap in direction within 95% confidence windows, demonstrating that the flow exposed on

the eastern side of the Godavari is most likely the same flow as the uppermost flow on the

western side of the river (Fig S9). Directions from Flow 2 and Flow 3 do not pass Watson's

V reversal test or the McFadden and McElhinny (1990) reversal test. This failure suggests

that significant time has passed between the eruption of the two flows and this is consistent

with geochronologic analysis (Section 2.3).

Table 1: *Summary of paleomagnetic results*

Site Name	Lat. (°N)	Long. (°E)	Geo Dec (°)	Geo Inc (°)	α95	n	k	R	VGP Lat (°)	VGP Lon (°)	Chron
Flow 1	17.0310	81.6345	158.7	78.6	5.2	7	137.6	6.91	-3.5	89.5	C29r
Flow 2	17.0270	81.6141	162.5	39.2	2.9	8	358.1	7.98	-47.2	105.8	C29r
Flow 3	17.0354	81.7146	301.1	-43.5	11.5	6	34.7	5.86	18.7	316.5	C29n

Note: Latitude and Longitude are the average Lat/Lon from samples locations of each flow based on the World Geodetic System 1984 (WGS84) datum. Geo dec/inc indicate declination/inclination of characteristic remanent directions in geographic coordinates determined using Fisher statistics (Fisher, 1953). R is resultant vector; *k* is the precision parameter; α95 is the 95% confidence interval of the Fisher mean; VGP lat/lon are the latitudes and longitudes of the virtual geomagnetic poles.

2.3 ^{40}Ar/^{39}Ar dating

Samples of the three exposed flows were subjected to ^{40}Ar/^{39}Ar analysis of

plagioclase separates at the BGC using facilities and methods described by Sprain et al.

(2019). We sampled the lowest flow (sample RJ17-1) in 2017 and separated 297-595 µm plagioclase crystals; the middle (RA99.23) and upper (RA99.14) flows were splits (63-125 µm plagioclase crystals) of the same samples analyzed by Knight et al. (2003). In hand sample, plagioclase crystals from all flows were up to ~300-500 µm, so the grain sizes analyzed for the upper two flows are very likely groundmass plagioclase. A few tens of milligrams of plagioclase from the middle and upper flows were irradiated in the same batch and analyzed in four replicate incremental heating experiments, whereas a similar amount from the lower flow was irradiated separately and analyzed in only two incremental heating experiments (see Table S1 for complete data including J values, and Text S1 for detailed methods).

Apparent age spectra (Fig. 3a) for all samples yielded well-developed and concordant plateaux over >85% of the ^{39}Ar released. The lower flow (RJ17-1) yielded significantly higher and less consistent Ca/K values, >150 for all steps, whereas the middle and upper flows (RA99.23 and RA99.14, respectively) have Ca/K values that vary more consistently throughout the age spectra and are less than 50 in all steps (Fig. 3a).

Weighted (by inverse variance) mean plateau ages for the three flows based on our analyses are shown in Table 1. These new results are more precise than those reported by Knight et al. (2003), largely due to more precisely and accurately determined J-values obtained by densely bracketing unknowns with standards during irradiation. The previous results contribute negligibly to weighted mean ages (pooling our new data with those of Knight et al. (2003)), hence we refrain from combining results. Our ages preserve stratigraphic order, although the ages of the lower and middle flows are indistinguishable at the 1σ level. All ages were determined using the optimization model of Renne et al., (2010) and the calibration of Renne et al. (2011), and age uncertainties are reported at the 1σ level

stated as ± *x/y*, where *x* indicates analytical uncertainty and *y* indicates systematic uncertainty. Corrections were applied for mass discrimination, decay constants, and atmospheric argon (Text S1; Lee et al., 2006; Renne et al., 2009; Renne and Norman, 2001; Stoenner et al., 1965).

Based on these dates, the lower flow (65.916 ± 0.239/0.245 Ma) postdates the Cretaceous-Paleogene boundary as dated by ^{40}Ar/^{39}Ar at 66.052 ± 0.008/0.043 Ma (Sprain et al., 2018), although the dates are not distinguishable at the 1σ level (Fig S10). The poor age precision on this flow is due to its high Ca/K ratio, and we further constrain its chronology relative to the Cretaceous-Paleogene boundary using its geochemical formation assignment (Sections 2.5 and 3). The lower flow date is also not distinguishable with high confidence from the ^{40}Ar/^{39}Ar age for the end of geomagnetic polarity chron C29r (65.724 ±0.013/0.044 Ma; Sprain et al., 2018). At the 95% confidence level, the lower flow could have erupted as much as ~50 ka after the end of chron C29r, but the most probable inference is that it was emplaced in chron C29r, due to its reverse polarity.

The date for the middle flow (65.667 ± 0.065/0.079 Ma) is definitively younger than the Cretaceous-Paleogene boundary (separated by more than 2σ) (Fig. S10). Its reverse polarity constrains it to within chron C29r, and its date is not distinguishable from the chron C29r/C29n boundary at the 1σ level, despite the most likely age falling within C29n. Our age for the upper flow (65.265 ± 0.061/0.076 Ma) is well within the age span of chron C29n, consistent with its normal polarity (as reported in the Geologic Time Scale 2012; Ogg, 2012). It is noteworthy that the age of the upper flow is younger than any of the dated lava flows in the Western Ghat sequence (Sprain et al., 2019).

Table 2: *Summary of ^{40}Ar/^{39}Ar dates*

Flow	Sample	Age (Ma)	± σ (analytical)	± σ (systematic)

Upper	RA99.14	65.265	0.061	0.076
Middle	RA99.23	65.667	0.065	0.079
Lower	RJ17-1	65.916	0.239	0.245

2.4 Micropaleontology and biostratigraphy

2.4.1. Sampling procedures and identification of foraminifera: For

micropaleontological analysis, 17 samples across the carbonate intertrappean unit were
collected and studied in the Government Quarry section (Fig. 1; see Fig. 6 for detailed
stratigraphic placement of samples). Because all the samples were very lithified, to extract
foraminiferal specimens, we disaggregated around 200 grams per sample, using a solution
with 80% acetic acid and 20% H_2O for 4 hours. Samples were dried at $\leq 50^\circ C$ and then sieved
into 38-63 μm and ≤63μm size fractions. All specimens were identified, sorted, and fixed on
standard 60-square micropaleontological slides. We picked planktic foraminiferal specimens
and photographed them under the scanning electron microscopes Zeiss MERLIN FE-SEM at
the Electron Microscopy Service of the Universidad de Zaragoza (Spain). They are
illustrated in Fig. 4. For the biostratigraphic determinations, we have used the biozonations of
Berggren and Pearson (2005).

Micropaleontological assemblages of the carbonate intertrappean unit are composed
of marine to freshwater taxa, such as charophyte fructifications (gyrogonites), ostracods,
gastropods, bivalves, fish teeth, and foraminifers. Planktic/Benthic foraminiferal ratio is very
low in all the samples, around 1%. Benthic foraminifera include *Nonion, Cibicides,*
Dentalina, Protelphidium and miliolids. These and other genera have been previously
reported in this outcrop by Malarkodi et al. (2010), who estimated environments ranging
from shallow marine to brackish estuarine based on benthic foraminiferal and ostracode
assemblages. The planktic foraminifera are almost absent in our samples, and the

preservation of tests is generally very poor. Despite an intensive search, we could only find 14 specimens in the 17 samples studied (specifically in samples GQN3, 4, 7, 10, 11 and 12).

The identified Cretaceous species include *Heterohelix globulosa* (Figs. 4.1-3), *Heterohelix* aff. *globulosa* (transitional to *Heterohelix punctulata*; Figs. 4.4-5), *Globigerinelloides rosebudensis* (Fig. 4.6), *Pseudoguembelina costulata* (Fig. 4.7), and probably *Guembelitria cretacea* (Fig. 4.8). Among the Danian species, the following stand out: *Eoglobigerina trivialis* or *Subbotina triloculinoides* (Fig. 4.9), *Parasubbotina varianta* (Fig. 4.10), *Praemurica inconstans* (Fig. 4.11), and *Globoconusa* aff. *daubjergensis* (Figs. 4.12-13). A probable specimen (internal mold) of *Parasubbotina pseudobulloides* was also found (Fig. 4.14). These specimens belong to mixed assemblages of upper Cretaceous and Danian planktic foraminifera, and hence suggest an early Danian age for the carbonate intertrappean unit. Given the mixed assemblage, and that nearshore environments such as these are not inhabited by planktic foraminifera, we conclude the Cretaceous specimens must be considered reworked and that Danian specimens, if *in situ*, had to be transported from open ocean by postmortem displacement of tests due to surface water currents.

2.4.2. Biostratigraphic placement: Indubitable specimens of Danian index-species have not been identified. Nevertheless, although its gross morphology does not fit strictly, the *Eoglobigerina* or *Subbotina* specimen (Fig. 4.9) found in GQN10 could belong to *S. triloculinoides*, which is the index-species of Subzone P1b of Berggren and Pearson (2005). Its lowest occurrence is close to the C29r/C29n boundary (Berggren and Pearson, 2005) and, according to Arenillas et al. (2004), in the uppermost part of C29r. The lowest occurrence of *Gc. daubjergensis* is at the Subzone P1a (Arenillas et al., 2004), and its abundance is high in relatively shallow outer neritic environments (Olsson et al., 1999), mainly from the Subzone P1b. The identification of specimens closely related to this species (*Gc.* aff. *daubjergensis*) in

GQN3 and GQN10 indicates that the carbonate intertrappean unit could belong to Subzone P1a, but more likely to Subzone P1b. No species typical of the Zone Pα, such as *Parvularugoglobigerina eugubina*, and/or Subzone P1c, as *Globanomalina compressa*, have been found in the Government Quarry section.

The triserial specimen identified in GQN12 is poorly preserved but seems to belong to *G. cretacea*. *Guembelitri*a might be the only surviving planktic foraminiferal genus of the end-Cretaceous mass extinction (Smit et al., 1982; Arenillas and Arz, 2017). Nevertheless, the highest occurrence of the genus *Guembelitria* is in the lower part of Zone Pα, as has been recently proposed by Arenillas et al. (2018), and it is subsequently replaced by species of the genus *Chiloguembelitria* (Arenillas et al., 2017). If the carbonate intertrappean unit belongs to Subzone P1b, then the *G. cretacea* specimen found in GQN12 is reworked and probably Cretaceous in age.

2.5 Geochemistry of RT basalts and intertrappean sediments

Comparison of trace element data from previous studies of RT basalts including identified flows (Knight et al., 2003) with compiled chemical data for the main Deccan province (Vanderkluysen et al., 2011) indicates all of the RT flows are consistent with the Ambenali geochemical formation (Fig. 5), as previous studies have suggested (e.g., Baksi, 2001). However, the upper Mahabaleshwar Formation has previously been noted to have similar chemical characteristics to the Ambenali Formation (Cox and Hawkesworth, 1985; Devey and Lightfoot, 1986). For instance, lower to middle Mahabaleshwar flows have Zr/Nb ratios of 9-10, whereas Ambenali and upper Mahabaleshwar flows have Zr/Nb ≥ 11 (Jay, 2005). All three Rajahmundry flows have Zr/Nb ≥ 11 (Knight et al., 2003; Baksi, 2001). Therefore, given the uppermost flow's chemistry, normal polarity, and younger age, it is

better assigned to the Mahabaleshwar Fm. rather than the Ambenali. The Panhala Formation also has somewhat similar geochemistry and normal polarity, but its known spatial extent is restricted to a relatively small area within the Western Ghats (Lightfoot et al., 1990). Consequently, it is more likely that RT Flow 3 represents a distal exposure of the Mahabaleshwar Formation. Barium concentration in all three flows is high compared to Western Ghats Ambenali compositions, but this is presumably due to post-eruption interaction with seawater or marine sediments. This is corroborated by a covariation observed between strontium and oxygen isotope composition in Rajahmundry basalt samples, which indicates the strontium composition has been altered by seawater (Baksi, 2001). Baksi (2001) accounted for this relationship, calculating a primary $^{87}Sr/^{86}Sr$ value of 0.7040. This is consistent only with the values expected for the Ambenali and Mahabaleshwar Formations (0.7038-0.7044 and 0.7040-0.7055 respectively, Vanderkluysen et al., 2011). In summary, Flows 1 and 2 are most consistent with the Ambenali Formation, and Flow 3 with the upper Mahabaleshwar Formation.

We have analyzed the carbon isotope composition ($\delta^{13}C_{VPDB}$) of the carbonate intertrappean sediments between flows 1 and 2 (Fig. 6) in the Government Quarry section. We collected samples from fresh quarry exposures and stored them in plastic bags. In the lab, we drilled each sample to collect powder from carbonate matrix, taking care to avoid large fossils. We determined $\delta^{13}C$ and $\delta^{18}O$ values using a MultiCarb system in line with a GV IsoPrime mass spectrometer in Dual Inlet at the Center for Stable Isotope Biogeochemistry at UC Berkeley. NIST standard 8544 (NBS19) was analyzed (N=3, within 1% of accepted value, standard deviation of 0.025‰), as well as internal standards (N=4, standard deviation of 0.055‰).

The $\delta^{13}C_{VPDB}$ values of the intertrappean carbonate unit are between 1 and −7 ‰. Marine carbonates in the Cretaceous and Paleocene have a composition of approximately 0 to 2.5‰, thus the two points (samples GQN 5 and 8) in the interior of the carbonate unit which have $\delta^{13}C$ values within that range are broadly consistent with deposition in a shallow marine environment or near-shore carbonate platform (e.g., Lerman and Clauer, 2014 and references therein). However, the majority of the unit, especially near the base and top, has more negative $\delta^{13}C$ values of -4 to -7‰, indicating the carbon source may have been the cooling and degassing basalt, which presumably had a composition similar to the mantle (−5 to −7 ‰) (e.g., Lerman and Clauer, 2014 and references therein). The top of the intertrappean, which is independently hypothesized to be altered and recrystallized due to the overlying basalt flow (e.g., Keller et al., 2008), also has a of $\delta^{13}C$ value of ∼−7 ‰. Overall, it is likely that the carbon isotope composition of the carbonate unit dominantly reflects that of the basalt composition, whether due to post-depositional alteration or composition at time of formation.

3. Chronostratigraphy of Rajahmundry Traps

We conclude that all three exposed flows of the Rajahmundry Traps were emplaced in the Danian (Fig. 6). The reverse polarity of Flows 1 and 2 require emplacement during chron C29r, and the radioisotopic dates of 65.916 ± 0.239 Ma and 65.667 ± 0.065 Ma (±1σ, analytical) constrain them to post-Cretaceous-Paleogene boundary (66.052 ± 0.008 Ma, Sprain et al., 2018) in age. The date for Flow 1 is within uncertainty of the Cretaceous-Paleogene boundary, however its geochemical assignment to the Ambenali Formation also requires post-boundary emplacement (e.g. Sprain et al., 2019; Schoene et al., 2019). This is corroborated by the foraminifera in the carbonate intertrappean, which most closely align to Danian planktic foraminiferal Subzone P1b, consistent with deposition near the C29r/C29n

boundary. Flow 3, the uppermost flow, has a normal polarity, and a date of 65.265 ± 0.061 Ma, both of which are consistent with emplacement within chron C29n.

We can more precisely determine the timing of the lower two flows by combining the new RT ^{40}Ar/^{39}Ar dates and paleomagnetic constraints with the date of the C29r/C29n transition from Sprain et al. (2018). The convolution of the magnetic reversal age distribution (65.724 ± 0.044 Ma, Sprain et al., 2018) results in ages for Flow 1 of 65.916 ± 0.210 Ma and for Flow 2 of 65.706 ± 0.043 Ma (Text S2 and Fig. S8). These ages require that the carbonate intertrappean unit be deposited over a period of ~250 ka at most and the red bole over a period of ~400 ka. While ~2 m is a relatively small amount of alteration and/or sediment accumulation for ~400 ka, the red bole here is thicker than most boles within the Western Ghats (Widdowson et al., 1997). These ages are consistent with modern ^{40}Ar/^{39}Ar dates for the Ambenali and Mahabaleshwar Formations from the main Deccan province (Sprain et al., 2019). The RT have previously been geochemically correlated to these formations (Baksi, 2001; Jay and Widdowson, 2008; Knight et al., 2003; Manikyamba et al., 2015). Comparison of RT trace element data with a recent Deccan geochemistry compilation from Vanderkluysen et al. (2011) yields the same result (Fig. 5). As the Ambenali-Mahabaleshwar transition is within chron C29r in the MDVP (Vandamme and Courtillot, 1992), our chronostratigraphy – with the lower two flows belonging to the Ambenali Formation and the upper flow to the upper Mahabaleshwar Formation – demonstrates that the RT basalts are compatible with contemporaneous MDVP chemostratigraphy and magnetostratigraphy.

Given this compatibility, we can further constrain the timing of Flow 1 using its assignment to the Ambenali Formation. As Flow 1 cannot be older than the Poladpur to Ambenali composition transition, we convolve the age for Flow 1 with the youngest date for the Poladpur Formation from the Sprain et al. (2019) MDVP chronostratigraphy (65.940 ± 0.092 Ma). This calculation results in a most likely age for Flow 1 of 65.916 +0.096, –0.202

Ma (Fig. S8b). We emphasize that this is dependent on the assumption that the RT basalts are an extension of MDVP flows and that the geochemical formations are isochronous within the MDVP.

While the exposed flows are most likely all post-Cretaceous-Paleogene boundary in age, analysis of sub-surface cores from near the mouth of the Godavari river (approximately 50 km to the south of the Rajahmundry Traps), suggests the presence of up to 8 similarly sized lava flows from the late Maastrichtian onward (Keller et al., 2011). The exact number of flows varies between cores, presumably because of complex lava flow dynamics resulting in kipukas (areas uncovered by lava) and slightly different paths for each lava flow (e.g., Reynolds et al., 2017). This type of lava flow morphology is frequently due to even slight topographic features in the underlying sediment, and results in variation of flow thickness due to ensuing inflation (Self et al., 1998).

The age of the subsurface flows has been estimated based on biostratigraphic correlation of intertrappean sediments to planktic foraminiferal zones. The lower 3 or 4 flows have sediments between them within Zone CF1 (Keller et al., 2011, 2012), suggesting deposition within the last 110 ka of the Cretaceous (Coccioni and Premoli Silva, 2015). According to Keller et al. (2011), the upper 3 or 4 flows have intertrappean sediments which correlate to Subzones P1a and P1b of Keller et al. (1995), which are roughly equivalent respectively to Zone Pα and Subzone P1a of Berggren and Pearson (2005). The exposed Rajahmundry Traps flows may correlate with some of these Paleocene flows within the cores, and the regional tilt to the southeast accounts for the 2.5 to 3 km of overlying sediment in the cores. These large lava flows are broadly consistent with the geochronology of the Western Ghats, although there is no geochemical data available for the subsurface flows to correlate them to specific geochemical formations.

4. Discussion

4.1 Correlation with Deccan chemostratigraphy and implications for Rajahmundry Traps eruptive vents

The geochemistry of the RT has long been correlated broadly to a mantle plume source, and specifically to the Ambenali and Mahabaleshwar Formations of the Western Ghats (e.g., Baksi, 2001; Manikyamba et al., 2015). All three flows have trace element compositions broadly consistent with the Ambenali Formation (Fig. 5). While Flow 3 is significantly younger than the Ambenali Formation in the Western Ghats (e.g., Sprain et al., 2019), the upper Mahabaleshwar Formation has previously been found to have an Ambenali-like trace element composition (e.g., Lightfoot et al., 1990). The youngest date from the upper Mahabaleshwar Formation from the Western Ghats, which is also the youngest high-precision date from the MDVP, is ~65.42 Ma (Sprain et al., 2019). However, as this date is not from the top of the Mahabaleshwar Formation, it is entirely possible the emplacement of the Mahabaleshwar Formation continued for another ~150 ka until the emplacement of Flow 3 at 65.27 Ma. The Panhala Formation, which overlies the Mahabaleshwar Formation, is also geochemically similar to the upper Mahabaleshwar and Ambenali Formations (Lightfoot et al., 1990). Further work to date the boundary of the Mahabaleshwar and Panhala Formation boundary will enable a definitive formation assignment, however Mahabaleshwar is the more parsimonious choice, as the Panhala Formation is known from only a few places within the Main Deccan Volcanic Province. The new chronostratigraphy for the RT thus suggests that the chemistry of the RT flows is consistent with the contemporaneous Western Ghats geochemical formations.

The robust correlation with main province Deccan geochemistry has long led to the conclusion that the RT basalts erupted from the same vents as the Ambenali and Mahabaleshwar Formations (e.g., Baksi, 2001; Self et al., 2008). However, it has also been

hypothesized that the RT basalts are the result of local volcanism associated with rifting, although still affiliated with Deccan magma sources (Lakshminarayana et al., 2010; Manikyamba et al., 2015). This hypothesis is driven by potential lack of a clear down-slope pathway between the main Deccan province and Rajahmundry due to tectonic uplift of the Eastern Ghats (Lakshminarayana et al., 2010). We do not think this is likely, as there are no known intrusive magma bodies, sills, or dykes of appropriate age near Rajahmundry despite extensive basement exposures (e.g., Geological Survey of India, 2000a; 2000b). This is in contrast to other Deccan sub-provinces such as the Malwa Plateau, the Mandla Lobe, and the Kutch-Saurashtra region, which each have a large number of dikes compositionally similar to the lava flows (e.g., Vanderkluysen et al., 2011). Furthermore, all three RT flows are at least 20 meters thick, requiring a higher eruptive flux than is typically associated with smaller-scale fissure volcanism (e.g., Deschamps et al., 2014). Thus, the most parsimonious explanation remains that the RT basalts originated from some of the same eruptive centers as the Western Ghats lavas and flowed ~1000 km to the Rajahmundry area, even if their exact path is unknown (Fig 1; Self et al. 2008). By contrast, there are geochemical and volcanological reasons to suspect independent eruptive centers for the other Deccan sub-provinces (e.g., Kale et al., 2020).

Assuming the RT flows are an extension of the MDVP, the date for Flow 2 requires that large volume flows of Ambenali composition be erupted less than 100 ka prior to the C29r/C29n boundary. This is consistent with the Sprain et al. (2019) geochronologic framework for the Western Ghats, which describes a roughly uniform eruptive rate through the Deccan sequence. However, it is inconsistent with a hiatus of approximately 300 ka between the top of the Ambenali Formation and the C29r/C29n boundary, as suggested by Schoene et al. (2019). This suggests two possibilities: either the Ambenali Formation is not

isochronous between the RT and the Western Ghats (and within the Western Ghats), or the hiatus inferred by Schoene et al. (2019) is not uniform throughout the Main Deccan Volcanic Province. The RT chronology cannot resolve this in isolation; however, the consistency with the dates from the Sprain et al. (2019) chronology supports the latter.

4.2 Timing of Rajahmundry flows with respect to Cretaceous-Paleogene mass extinction and Danian climate change

Flood basalt eruptions have the potential to cause climate change due to emission of SO_2 and CO_2 (e.g., Schmidt et al., 2016; Self et al., 2006). Our chronostratigraphy of the Rajahmundry Traps shows that the three exposed flows were emplaced after the Cretaceous-Paleogene boundary and are therefore unrelated to the mass extinction, regardless of any potential climate consequences (Fig. 6). However, it confirms that large volume Deccan eruptions were occurring well into the Danian. It is therefore important to address whether these eruptions could have caused climate change and therefore perturbed ecosystems during the recovery interval.

Ecological community stability was highly variable for the first ~700 ka of the Paleocene, until ~65.3 Ma (Alvarez et al., 2019; see also Birch et al., 2016; Smith et al., 2018). There are several periods of climate change during this time interval, including the Danian-C2 (Dan-C2) and lower-C29n hyperthermal events (Coccioni et al., 2010; Dinarès-Turell et al., 2014). The former is a double-peaked warming event, with total duration of approximately 100 ka and which terminated at the C29r/C29n transition, while the latter occurred approximately ~100 ka later at ~65.6 Ma, near the base of chron C29n (e.g., Coccioni et al., 2010; Coccioni et al., 2012, Dinarès-Turell et al., 2014; Sinnesael et al., 2019). Both are associated with small decreases (<1‰) in benthic carbon isotope composition, although the global nature of both events is debated (e.g., Barnet et al., 2019;

Sinnesael et al., 2019). The RT flows all occurred within this 700-ka period of highest amplitude variability in community stability. Furthermore, Flows 1 and 2 were erupted around the same time as the Dan-C2 hyperthermal event (Fig 7).

To test whether the eruptive CO_2 emissions of these voluminous flows could have directly caused observable warming, we estimated the effects of these emissions on the atmosphere and ocean. To do this, we used scaling relationships from an intermediate complexity Earth system model (LOSCAR, Zeebe, 2012) to estimate the peak changes in atmospheric carbon (pCO_2) and temperature as a response to volcanogenic CO_2 input forcing (Towles et al., 2015). The LOSCAR model has been used previously to model the climate effects of Deccan Traps and North Atlantic Igneous Province CO_2 emissions (e.g., Hull et al., 2020; Zeebe, 2012).

The volcanogenic CO_2 input forcing is parameterized as a triangular shaped emission history with a specified duration and total amount emitted (Towles et al., 2015). We relate the CO_2 emissions to a volume of erupted basalt using an estimated Deccan basalt CO_2 content of 0.5 weight percent, or 14 Tg CO_2 per km^3 (Self et al., 2006, see also Capriolo et al., 2020). We used the change in atmospheric pCO_2 for each emissions history to calculate the consequent change in atmospheric temperature using a given equilibrium climate sensitivity (°C per pCO_2 doubling, see Zeebe, 2012 equation 51). We then estimated the temperature change in the deep ocean using the scaling relationship between atmospheric and ocean temperature changes for a given emission scenario from Towles et al. (2015). This process enabled us to estimate the temperature change in the deep ocean caused by volcanic CO_2 emissions for a variety of eruption sizes and durations. We can also assess the roles of different initial atmospheric pCO_2 concentrations and equilibrium climate sensitivity values. In the early Paleocene, background pCO_2 is estimated to be ~300-600 ppm (Milligan et al.,

2019), and equilibrium climate sensitivity in the ice-free early Paleocene is estimated to be 3°C per pCO_2 doubling (Royer, 2016).

We find that it is difficult to cause $\geq$ 2°C warming with the volcanogenic CO_2 emissions expected for a Rajahmundry-scale Deccan eruption ($\sim$5000 km^3), even given a sensitive set of initial conditions. Using a low initial pCO_2 concentration of 300 ppm and a high climate sensitivity of 4 °C per pCO_2 doubling, 2°C of warming corresponds with $\sim$100,000 km^3 basalt erupted within at most a few (1-3) thousand years (Fig. 8a). An eruptive pulse of this size shortly before the chron C29r/C29n boundary is inconsistent with both proposed Deccan age models for the Main Deccan Volcanic Province (Schoene et al., 2019; Sprain et al., 2019). For reference, this volume is much larger than the total volume of each of the other Deccan sub-provinces (e.g., Malwa Plateau $\sim$ 21,000 km^3, Schöbel et al., 2014). The required eruptive rate is also much higher than the estimates of 10 km^3/year during the pulses described in the Schoene et al., (2019) age model. Hence, magmatic CO_2 emissions associated with RT flow eruptions, or any other individual Deccan eruption, are unlikely to have directly caused significant climate warming, including the Dan-C2 and Lower-C29n warming events.

Utilizing more standard initial conditions (an initial pCO_2 of 450 ppm and climate sensitivity of 3°C per pCO_2 doubling), we expect each RT eruption to have instead caused $\sim$0.1-0.2°C of warming (Fig. 8b). The extent of warming depends on the duration of each eruption, which we estimate is 50-500 years for the Deccan Traps (Fendley et al., 2019). Additionally, the upper estimate of eruptive rates suggests RT eruptions potentially caused volcanogenic sulfate aerosol driven cooling of greater than 2°C (Fig. 8, Schmidt et al., 2016; Self et al., 2006). However, given the short lifetime of sulfate aerosols in the atmosphere, this cooling would persist only during the active eruption, while elevated CO_2 could last for

thousands of years (e.g., Black et al., 2018; Schmidt et al., 2016). The short duration of volcanogenic cooling means it is unlikely to be recorded in paleoclimate records of ~1000-year resolution (e.g., Barnet et al., 2019; Black et al., 2018).

Other warming events typically associated with the Deccan Traps, such as the Late Maastrichtian Warming Event, also have an amplitude of warming much greater than expected based on the erupted volume of basalt (e.g., Sprain et al., 2019; Hull et al., 2020). This suggests that that the climate impact of the RT flows, and other Deccan eruptions, was potentially amplified by environmental feedbacks. For instance, the Dan-C2 event has been hypothesized to be a combined consequence of Deccan CO_2 emissions and the first 405-ka eccentricity maximum of the Paleocene (Barnet et al., 2019; Sinnesael et al., 2019). Additionally, perturbations to large carbon reservoirs, such as the ocean and terrestrial environments (~60 and ~10 times more carbon than in the atmosphere respectively), can significantly affect atmospheric CO_2 concentration (e.g., Friedlingstein et al., 2019). Large volcanic eruptions can cause significant changes to these reservoirs through changes in ocean circulation and global precipitation (e.g., Black et al., 2018). These processes are challenging to parametrize and are not explicitly included in the LOSCAR model (Zeebe, 2012). Finally, the observed warming only lasts for less than 100 ka – too rapid for simple silicate weathering feedbacks to remove the added volcanogenic CO_2 from the atmosphere, even with enhanced basalt weathering (e.g., Hull et al., 2020). This suggests other environmental feedbacks may be involved in these brief hyperthermal events.

Additionally, measurements of CO_2 emissions from modern volcanic systems show that the passive (fumarolic, vent, and soil) degassing of CO_2 from intrusive magma bodies is significantly greater in magnitude (~100 x) than the amount of CO_2 released during eruptions (e.g., Fischer & Aiuppa, 2020; Mittal & Richards, 2019). If this is the case for the Deccan

volcanic system, then the total quantity of CO_2 emitted may be much larger than estimated from erupted volume alone. As the total Deccan eruptive interval lasted for ~ 1 Ma (e.g., Sprain et al., 2019), one may not expect a strong time dependence between the passively degassed CO_2 and the emplacement of the RT flows. However, a highly active magmatic system producing highly voluminous lava flows will likely also emplace large amounts of magma in the middle and upper crust. This process may consequently increase passive degassing concomitant with the RT eruptions.

In summary, we cannot conclusively determine if the RT eruptions caused global climate change. However, we can clearly show that eruptive CO_2 emissions were insufficient to directly cause multi-degree warming. Nevertheless, the relative timing of the RT flows suggests the Deccan Traps may have influenced marine and terrestrial ecological recovery, whether through climate change or other environmental effects (e.g., Smith et al. 2018; Lyson et al. 2019).

5. Conclusions

We have described a new chronostratigraphy for the exposed portion of the Rajahmundry Traps. These three Deccan lava flows are located approximately 400 km from any other known Deccan outcrop (Baksi, 2001), and nearly 1000 km to the east of the main Deccan eruptive centers in the Western Ghats. The great distance between these basalts and their hypothesized eruptive vents has led to their description as the distal ends of the longest known lava flows on Earth (Self et al., 2008). New $^{40}Ar/^{39}Ar$ dates, magnetostratigraphy, and biostratigraphy demonstrate that all three flows exposed were emplaced in the Danian, significantly after the end-Cretaceous mass extinction. The lower two flows are within magnetochron C29r, and the middle flow was emplaced close to the C29r/C29n transition. The uppermost flow was emplaced several hundred thousand years later, in C29n.

Our results are consistent with previous studies which place the Rajahmundry flows near the chron C29r/C29n boundary (e.g., Baksi, 2001; Knight et al., 2003). If these flows are derived from the MDVP, Flow 3 is the youngest recently dated Deccan lava flow (at 65.27 Ma), indicating that the Deccan Traps were erupting large volumes of basalt more than 700 thousand years into the Paleocene. The RT chronology confirms that the RT flows are coeval and geochemically consistent with the Western Ghats Ambenali and Mahabaleshwar chemostratigraphic formations. The middle RT flow's date, geochemistry, and magnetic polarity requires Ambenali-composition basalt to be erupted just prior to the C29n/C29r boundary. This is inconsistent with the last Ambenali composition flows erupting nearly 300 thousand years prior to the chron boundary, as has been proposed (Schoene et al., 2019). The RT chronology therefore implies that this hiatus is not uniformly present through the entire Deccan Traps, or that the Ambenali Fm. is not an isochronous unit. Resolving this inconsistency and verifying the synchronicity of the geochemical formations are thus priorities for future work.

As the timing of these flows suggests possible implications for ecological recovery, we test whether these large volume eruptions could have caused observable warming. Utilizing an intermediate complexity carbon cycle model (LOSCAR), we clearly show that eruptive CO_2 emissions were insufficient to directly cause multi-degree warming. However, environmental feedbacks (e.g., astronomical forcing) and/or non-eruptive volcanic CO_2 emissions may increase the climatic effects of the voluminous RT flows. If so, the timing of these flows suggests any disturbance may have impacted the protracted ecological recovery from the end-Cretaceous mass extinction.

References:

Alvarez, S. A., Gibbs, S. J., Bown, P. R., Kim, H., Sheward, R. M., & Ridgwell, A. (2019). Diversity decoupled from ecosystem function and resilience during mass extinction recovery. *Nature*, *574*(7777), 242–245. https://doi.org/10.1038/s41586-019-1590-8

Arenillas, I., & Arz, J. A. (2017). Benthic origin and earliest evolution of the first planktonic foraminifera after the Cretaceous/Palaeogene boundary mass extinction. *Historical Biology*, *29*(1), 25–42. https://doi.org/10.1080/08912963.2015.1119133

Arenillas, I., Arz, J. A., & Gilabert, V. (2017). Revalidation of the genus *Chiloguembelitria* Hofker: Implications for the evolution of early Danian planktonic foraminifera. *Journal of African Earth Sciences*, *134*, 435–456. https://doi.org/10.1016/j.jafrearsci.2017.07.011

Arenillas, I., Arz, J. A., & Gilabert, V. (2018). Blooms of aberrant planktic foraminifera across the K/Pg boundary in the Western Tethys: causes and evolutionary implications. *Paleobiology*, *44*(3), 460–489. https://doi.org/10.1017/pab.2018.16

Arenillas, I., Arz, J., & Molina, E. (2004). A new high-resolution planktic foraminiferal zonation and subzonation for the lower Danian. *Lethaia*, *37*(1), 79–95. https://doi.org/10.1080/00241160310005097

Baksi, A. K. (2001). The Rajahmundry Traps, Andhra Pradesh: Evaluation of their petrogenesis relative to the Deccan Traps. *Journal of Earth System Science*, *110*(4), 397–407. https://doi.org/10.1007/BF02702903

Baksi, A. K., Byerly, G. R., Chan, L.-H., & Farrar, E. (1994). Intracanyon flows in the Deccan province, India? Case history of the Rajahmundry Traps. *Geology*, *22*(7), 605–608. https://doi.org/10.1130/0091-7613(1994)022<0605:IFITDP>2.3.CO;2

Barnet, J. S. K., Littler, K., Westerhold, T., Kroon, D., Leng, M. J., Bailey, I., et al. (2019). A High-Fidelity Benthic Stable Isotope Record of Late Cretaceous–Early Eocene Climate Change and Carbon-Cycling. *Paleoceanography and Paleoclimatology*, *34*, 672-691. https://doi.org/10.1029/2019PA003556

Beane, J. E., Turner, C. A., Hooper, P. R., Subbarao, K. V, & Walsh, J. N. (1986). Stratigraphy, composition and form of the Deccan Basalts, Western Ghats, India. *Bulletin of Volcanology*, *48*, 61–83. https://doi.org/10.1007/BF01073513

Berggren, W. A., & Pearson, P. N. (2005). A revised tropical to subtropical Paleogene planktonic foraminiferal zonation. *Journal of Foraminiferal Research*, *35*(4), 279–298. https://doi.org/10.2113/35.4.279

Besse, J., & Courtillot, V. (2002). Apparent and true polar wander and the geometry of the geomagnetic field over the last 200 Myr. *Journal of Geophysical Research: Solid Earth*, *107*(B11), EPM 6-1-EPM 6-31. https://doi.org/10.1029/2000JB000050

Bhalla, S. N. (1966). Foraminifera from the Infra-Trappean Beds of the Pangadi Area, India. *Journal of Paleontology*, *40*(2), 343–353. Retrieved from http://www.jstor.org/stable/1301666

Birch, H. S., Coxall, H. K., Pearson, P. N., Kroon, D., & Schmidt, D. N. (2016). Partial collapse of the marine carbon pump after the Cretaceous-Paleogene boundary. *Geology*, *44*(4), 287–290. https://doi.org/10.1130/G37581.1

Black, B. A., Neely, R. R., Lamarque, J. F., Elkins-Tanton, L. T., Kiehl, J. T., Shields, C. A., et al. (2018). Systemic swings in end-Permian climate from Siberian Traps carbon and sulfur outgassing. *Nature Geoscience, 11*, 949–954. https://doi.org/10.1038/s41561-018-0261-y

Blandford, W. T. (1867). On the traps and intertrappean beds of western and central India. *Memoirs of the Geological Survey of India*, *6*, 137–162.

Capriolo, M., Marzoli, A., Aradi, L. E., Callegaro, S., Dal Corso, J., Newton, R. J., et al. (2020). Deep CO2 in the end-Triassic Central Atlantic Magmatic Province. *Nature Communications*, *11*(1), 1670. https://doi.org/10.1038/s41467-020-15325-6

Coccioni, R., Bancalà, G., Catanzarit, R., Fornaciari, E., Frontalini, F., Giusberti, L., et al. (2012). An integrated stratigraphic record of the Palaeocene–lower Eocene at Gubbio (Italy): new insights into the early Palaeogene hyperthermals and carbon isotope excursions. *Terra Nova*, *24*(5), 380–386. https://doi.org/10.1111/j.1365-3121.2012.01076.x

Coccioni, R., Frontalini, F., Bancalà, G., Fornaciari, E., Jovane, L., & Sprovieri, M. (2010). The Dan-C2 hyperthermal event at Gubbio (Italy): Global implications, environmental effects, and cause(s). *Earth and Planetary Science Letters*, *297*(1), 298–305. https://doi.org/10.1016/j.epsl.2010.06.031

Coccioni, R., & Premoli Silva, I. (2015). Revised Upper Albian–Maastrichtian planktonic foraminiferal biostratigraphy and magneto-stratigraphy of the classical Tethyan Gubbio section (Italy). *Newsletters on Stratigraphy*, *48*(1), 47–90. https://doi.org/10.1127/nos/2015/0055

Cox, K. G., & Hawkesworth, C. J. (1985). Geochemical Stratigraphy of the Deccan Traps at Mahabaleshwar, Western Ghats, India, with Implications for Open System Magmatic Processes. *Journal of Petrology*, *26*(2), 355–377. https://doi.org/10.1093/petrology/26.2.355

Devey, C. W., & Lightfoot, P. C. (1986). Volcanological and tectonic control of stratigraphy and structure in the western Deccan traps. *Bulletin of Volcanology*, *48*(4), 195–207. https://doi.org/10.1007/BF01087674

Deschamps, A., Grigné, C., Le Saout, M., Soule, S. A., Allemand, P., Van Vliet-Lanoe, B., & Floc'h, F. (2014). Morphology and dynamics of inflated subaqueous basaltic lava flows. *Geochemistry, Geophysics, Geosystems*, *15*(6), 2128–2150. https://doi.org/10.1002/2014GC005274

Dinarès-Turell, J., Westerhold, T., Pujalte, V., Röhl, U., & Kroon, D. (2014). Astronomical calibration of the Danian stage (Early Paleocene) revisited: Settling chronologies of sedimentary records across the Atlantic and Pacific Oceans. *Earth and Planetary Science Letters*, *405*, 119–131. https://doi.org/10.1016/j.epsl.2014.08.027

Fendley, I. M., Mittal, T., Sprain, C. J., Marvin-DiPasquale, M., Tobin, T. S., & Renne, P. R. (2019). Constraints on the volume and rate of Deccan Traps flood basalt eruptions using a combination of high-resolution terrestrial mercury records and geochemical box models. *Earth and Planetary Science Letters*, *524*, 115721. https://doi.org/https://doi.org/10.1016/j.epsl.2019.115721

Fischer, T. P., & Aiuppa, A. (2020). AGU Centennial Grand Challenge: Volcanoes and Deep Carbon Global CO2 Emissions From Subaerial Volcanism—Recent Progress and Future Challenges. *Geochemistry, Geophysics, Geosystems*, *21*(3), e2019GC008690. https://doi.org/10.1029/2019GC008690

Fisher, R. A. (1953). Dispersion on a sphere. *Proceedings of the Royal Society of London. Series A. Mathematical and Physical Sciences*, *217*(1130), 295–305. https://doi.org/10.1098/rspa.1953.0064

Friedlingstein, P., Jones, M. W., O'Sullivan, M., Andrew, R. M., Hauck, J., Peters, G. P., et al. (2019). Global Carbon Budget 2019. *Earth System Science Data*, *11*(4), 1783–1838. https://doi.org/10.5194/essd-11-1783-2019

Geological Survey of India. (2000a). District Resource Map, East Godavari District, Andhra Pradesh.

Geological Survey of India. (2000b). District Resource Map, West Godavari District, Andhra Pradesh.

Ghosh, P., Sayeed, M. R. G., Islam, R., & Hundekari, S. M. (2006). Inter-basaltic clay (bole bed) horizons from Deccan traps of India: Implications for palaeo-weathering and palaeo-climate during Deccan volcanism. *Palaeogeography, Palaeoclimatology, Palaeoecology*, *242*(1), 90–109. https://doi.org/https://doi.org/10.1016/j.palaeo.2006.05.018

Hull, P. M., Bornemann, A., Penman, D. E., Henehan, M. J., Norris, R. D., Wilson, P. A., et al. (2020). On impact and volcanism across the Cretaceous-Paleogene boundary. *Science*, *367*(6475), 266 LP – 272. https://doi.org/10.1126/science.aay5055

Jay, A. E., Niocaill, C. Mac, Widdowson, M., Self, S., & Turner, W. (2009). New palaeomagnetic data from the Mahabaleshwar Plateau, Deccan Flood Basalt Province, India: implications for the volcanostratigraphic architecture of continental flood basalt provinces. *Journal of the Geological Society*, *166*(1), 13–24. https://doi.org/10.1144/0016-76492007-150

Jay, A. E. (2005). *Volcanic architecture of the Deccan Traps, western Maharashtra, India: an integrated chemostratigraphic and paleomagnetic study [Ph.D. Dissertation]*. The Open University.

Jay, A. E., & Widdowson, M. (2008). Stratigraphy, structure and volcanology of the SE Deccan continental flood basalt province: implications for eruptive extent and volumes. *Journal of the Geological Society*, *165*(1), 177–188. https://doi.org/10.1144/0016-76492006-062

Kale, V. S., Dole, G., Shandilya, P., & Pande, K. (2020). Stratigraphy and correlations in Deccan Volcanic Province, India: Quo vadis? *Geological Society of America Bulletin*, *132*(3–4), 588–607. https://doi.org/10.1130/B35018.1

Keller, G., Adatte, T., Bhowmick, P. K., Upadhyay, H., Dave, A., Reddy, A. N., & Jaiprakash, B. C. (2012). Nature and timing of extinctions in Cretaceous-Tertiary planktic foraminifera preserved in Deccan intertrappean sediments of the Krishna–Godavari Basin, India. *Earth and Planetary Science Letters*, *341–344*, 211–221. https://doi.org/10.1016/j.epsl.2012.06.021

Keller, G., Adatte, T., Gardin, S., Bartolini, A., & Bajpai, S. (2008). Main Deccan volcanism phase ends near the K-T boundary: Evidence from the Krishna-Godavari Basin, SE India. *Earth and Planetary Science Letters*, *268*(3–4), 293–311. https://doi.org/10.1016/j.epsl.2008.01.015

Keller, G., Bhowmick, P. K., Upadhyay, H., Dave, A., Reddy, A. N., Jaiprakash, B. C., & Adatte, T. (2011). Deccan volcanism linked to the Cretaceous-Tertiary boundary mass extinction: New evidence from ONGC wells in the Krishna-Godavari Basin. *Journal of the Geological Society of India*, *78*(5), 399–428. https://doi.org/10.1007/s12594-011-0107-3

Keller, G., Li, L., & MacLeod, N. (1996). The Cretaceous/Tertiary boundary stratotype section at El Kef, Tunisia: how catastrophic was the mass extinction? *Palaeogeography, Palaeoclimatology, Palaeoecology*, *119*(3), 221–254. https://doi.org/10.1016/0031-0182(95)00009-7

Kirschvink, J. L. (1980). The least-squares line and plane and the analysis of palaeomagnetic data. *Geophysical Journal International*, *62*(3), 699–718. https://doi.org/10.1111/j.1365-246X.1980.tb02601.x

Knight, K. B., Renne, P. R., Halkett, A., & White, N. (2003). 40Ar/39Ar dating of the Rajahmundry Traps, Eastern India and their relationship to the Deccan Traps. *Earth and Planetary Science Letters*, *208*(1–2), 85–99. https://doi.org/10.1016/S0012-821X(02)01154-8

Krivolutskaya, N. A., & Kedrovskaya, T. B. (2020). Structure and Composition of the Nadayansky Lava Flow: an Example of the Homogeneity of Lava Flows of the Siberian Trap Province. *Geochemistry International*, *58*(4), 363–376. https://doi.org/10.1134/S0016702920040047

Lakshminarayana, G., Manikyamba, C., Khanna, T. C., Kanakdande, P. P., & Raju, K. (2010). New observations on Rajahmundry Traps of the Krishna-Godavari Basin. *Journal of the Geological Society of India*, *75*(6), 807–819. https://doi.org/10.1007/s12594-010-0071-3

Lerman, A., & Clauer, N. (2014). 9.16 - Stable Isotopes in the Sedimentary Record. In H. D. Holland & K. K. B. T.-T. on G. (Second E. Turekian (Eds.) (pp. 437–481). Oxford: Elsevier. https://doi.org/10.1016/B978-0-08-095975-7.00716-6

Lightfoot, P. C., Hawkesworth, C. J., Devey, C. W., Rogers, N. W., & Calsteren, P. W. C. V. A. N. (1990). Source and Differentiation of Deccan Trap Lavas: Implications of Geochemical and Mineral Chemical Variations. *Journal of Petrology*, *31*(5), 1165–1200. https://doi.org/10.1093/petrology/31.5.1165

Lyson, T. R., Miller, I. M., Bercovici, A. D., Weissenburger, K., Fuentes, A. J., Clyde, W. C., et al. (2019). Exceptional continental record of biotic recovery after the Cretaceous–Paleogene mass extinction. *Science*, *366*(6468), 977 LP – 983. https://doi.org/10.1126/science.aay2268

Mahoney, J. J. (1988). Deccan Traps. In J. D. Macdougall (Ed.), *Continental Flood Basalts* (pp. 151–194). Dordrecht: Springer Netherlands. https://doi.org/10.1007/978-94-015-7805-9_5

Mallick, S., Bardhan, S., Das, S. S., Paul, S., & Goswami, P. (2014). Naticid drilling predation on gastropod assemblages across the K–T boundary in Rajahmundry, India: New evidence for escalation hypothesis. *Palaeogeography, Palaeoclimatology, Palaeoecology*, *411*, 216–228. https://doi.org/https://doi.org/10.1016/j.palaeo.2014.07.001

Malarkodi, N., Keller, G., Fayazudeen, P. J., & Mallikarjuna, U. B. (2010). Foraminifera from the early Danian intertrappean beds in Rajahmundry quarries, Andhra Pradesh. *Journal of the Geological Society of India*, *75*(6), 851–863. https://doi.org/10.1007/s12594-010-0066-0

Manikyamba, C., Ganguly, S., Santosh, M., Saha, A., & Lakshminarayana, G. (2015). Geochemistry and petrogenesis of Rajahmundry trap basalts of Krishna-Godavari Basin, India. *Geoscience Frontiers*, *6*(3), 437–451. https://doi.org/10.1016/j.gsf.2014.05.003

McDonough, W. F., & Sun, S. -s. (1995). The composition of the Earth. *Chemical Geology*, *120*(3), 223–253. https://doi.org/https://doi.org/10.1016/0009-2541(94)00140-4

McFadden, P. L., & McElhinny, M. W. (1990). Classification of the reversal test in palaeomagnetism. *Geophysical Journal International*, *103*(3), 725–729. https://doi.org/10.1111/j.1365-246X.1990.tb05683.x

Milligan, J. N., Royer, D. L., Franks, P. J., Upchurch, G. R., & McKee, M. L. (2019). No Evidence for a Large Atmospheric CO2 Spike Across the Cretaceous-Paleogene Boundary. *Geophysical Research Letters*, *46*(6), 3462–3472. https://doi.org/10.1029/2018GL081215

Mittal, T., & Richards, M. A. (2019). Volatile Degassing From Magma Chambers as a Control on Volcanic Eruptions. *Journal of Geophysical Research: Solid Earth*, *124*(8), 7869–7901. https://doi.org/10.1029/2018JB016983

Mukherjee, S., Bardhan, S., Mallick, S., Paul, S., & Das, S. S. (2013). Intense Naticid drilling predation on Turritelline gastropods from below the K-T boundary at Rajahmundry, India. *PALAIOS*, *28*(10), 683–696. https://doi.org/10.2110/palo.2013.p13-007r

Ogg, J. G. (2012). Chapter 5 - Geomagnetic Polarity Time Scale. In F. M. Gradstein, J. G. Ogg, M. D. Schmitz, & G. M. B. T.-T. G. T. S. Ogg (Eds.), *The Geologic Time Scale 2012* (pp. 85–113). Boston: Elsevier. https://doi.org/10.1016/B978-0-444-59425-9.00005-6

Olsson, R. K., Berggren, W. A., Hemleben, C., & Huber, B. T. (1999). Atlas of Paleocene planktonic foraminifera. *Smithsonian Contributions to Paleobiology*.

Raja Rao, C.S., Sahasrabudhe, Y.S., Deshmukh, S.S. and Raman R.R. (1978). Distribution, structure and Petrography of the Deccan traps. *Records of the Geological Survey of India,* pp 1–43.

Renne, P. R., Balco, G., Ludwig, K. R., Mundil, R., & Min, K. (2011). Response to the comment by WH Schwarz et al. on "Joint determination of 40K decay constants and

40Ar∗/40K for the Fish Canyon sanidine standard, and improved accuracy for 40Ar/39Ar geochronology" by PR Renne et al.(2010). *Geochimica et Cosmochimica Acta*, *75*(17), 5097–5100. https://doi.org/10.1016/j.gca.2011.06.021

Renne, P. R., Cassata, W. S., & Morgan, L. E. (2009). The isotopic composition of atmospheric argon and 40Ar/39Ar geochronology: Time for a change? *Quaternary Geochronology*, *4*(4), 288–298. https://doi.org/10.1016/j.quageo.2009.02.015

Renne, P. R., & Norman, E. B. (2001). Determination of the half-life of 37Ar by mass spectrometry. *Physical Review C*, *63*(4), 47302. https://doi.org/10.1103/PhysRevC.63.047302

Renne, P. R., Sprain, C. J., Richards, M. A., Self, S., Vanderkluysen, L., & Pande, K. (2015). State shift in Deccan volcanism at the Cretaceous-Paleogene boundary, possibly induced by impact. *Science*, *350*(6256), 76–78. https://doi.org/10.1126/science.aac7549

Reynolds, P., Holford, S., Schofield, N., & Ross, A. (2017). Three-Dimensional Seismic Imaging of Ancient Submarine Lava Flows: An Example From the Southern Australian Margin. *Geochemistry, Geophysics, Geosystems*, *18*(11), 3840–3853. https://doi.org/10.1002/2017GC007178

Sahu, H. S., Raab, M. J., Kohn, B. P., Gleadow, A. J. W., & Bal, K. D. (2013). Thermal history of the Krishna–Godavari basin, India: Constraints from apatite fission track thermochronology and organic maturity data. *Journal of Asian Earth Sciences*, *73*, 1–20. https://doi.org/10.1016/j.jseaes.2013.04.028

Schmidt, A., Skeffington, R. A., Thordarson, T., Self, S., Forster, P. M., Rap, A., et al. (2016). Selective environmental stress from sulphur emitted by continental flood basalt eruptions. *Nature Geoscience*, *9*(1), 77–82. https://doi.org/10.1038/ngeo2588

Schöbel, S., de Wall, H., Ganerød, M., Pandit, M. K., & Rolf, C. (2014). Magnetostratigraphy and 40Ar–39Ar geochronology of the Malwa Plateau region (Northern Deccan Traps), central western India: Significance and correlation with the main Deccan Large Igneous Province sequences. *Journal of Asian Earth Sciences*, *89*, 28–45. https://doi.org/10.1016/j.jseaes.2014.03.022

Schoene, B., Eddy, M. P., Samperton, K. M., Keller, C. B., Keller, G., Adatte, T., & Khadri, S. F. R. (2019). U-Pb constraints on pulsed eruption of the Deccan Traps across the end-Cretaceous mass extinction. *Science*, *363*(6429), 862 LP – 866. https://doi.org/10.1126/science.aau2422

Self, S., Jay, A. E., Widdowson, M., & Keszthelyi, L. P. (2008). Correlation of the Deccan and Rajahmundry Trap lavas: Are these the longest and largest lava flows on Earth? *Journal of Volcanology and Geothermal Research*, *172*(1–2), 3–19. https://doi.org/10.1016/j.jvolgeores.2006.11.012

Self, S., Keszthelyi, L., & Thordarson, T. (1998). The Importance of Pahoehoe. *Annual Review of Earth and Planetary Sciences*, *26*(1), 81–110. https://doi.org/10.1146/annurev.earth.26.1.81

Self, S., Widdowson, M., Thordarson, T., & Jay, A. E. (2006). Volatile fluxes during flood basalt eruptions and potential effects on the global environment: A Deccan perspective. *Earth and Planetary Science Letters*, *248*(1–2), 517–531. https://doi.org/10.1016/j.epsl.2006.05.041

Sen, B., & Sabale, A. B. (2011). Flow-types and lava emplacement history of Rajahmundry Traps, west of River Godavari, Andhra Pradesh. *Journal of the Geological Society of India*, *78*(5), 457–467. https://doi.org/10.1007/s12594-011-0111-7

Sinnesael, M., Montanari, A., Frontalini, F., Coccioni, R., Gattacceca, J., Snoeck, C., et al. (2019). Multiproxy Cretaceous-Paleogene boundary event stratigraphy: An Umbria-Marche basinwide perspective. In C. Koeberl & D. M. Bice (Eds.), *250 Million Years of Earth History in Central Italy: Celebrating 25 Years of the Geological Observatory of Coldigioco*. (Vol. 542, pp. 133–158). Geological Society of America Special Paper. https://doi.org/10.1130/2019.2542(07)

Smit, J. (1982). Extinction and evolution of planktonic foraminifera after a major impact at the Cretaceous/Tertiary boundary. In L. T. Silver & P. H. Schultz (Eds.), *Geological implications of impacts of large asteroids and comets on the earth* (Vol. 190, pp. 329–352). Geological Society of America Special Paper. https://doi.org/10.1130/SPE190-p329

Smith, S. M., Sprain, C. J., Clemens, W. A., Lofgren, D. L., Renne, P. R., & Wilson, G. P. (2018). Early mammalian recovery after the end-Cretaceous mass extinction: A high-resolution view from McGuire Creek area, Montana, USA. *Geological Society of America Bulletin*, *130*(11–12), 2000–2014. https://doi.org/10.1130/B31926.1

Sprain, C. J., Renne, P. R., Clemens, W. A., & Wilson, G. P. (2018). Calibration of chron C29r: New high-precision geochronologic and paleomagnetic constraints from the Hell Creek region, Montana. *Geological Society of America Bulletin*, *130*(9–10), 1615–1644. https://doi.org/10.1130/B31890.1

Sprain, C. J., Renne, P. R., Vanderkluysen, L., Pande, K., Self, S., & Mittal, T. (2019). The eruptive tempo of Deccan volcanism in relation to the Cretaceous-Paleogene boundary. *Science*, *363*(6429), 866 LP – 870. https://doi.org/10.1126/science.aav1446

Stoenner, R. W., Schaeffer, O. A., & Katcoff, S. (1965). Half-Lives of Argon-37, Argon-39, and Argon-42. *Science*, *148*(3675), 1325 LP – 1328. https://doi.org/10.1126/science.148.3675.1325

Subbarao, K. V, & Pathak, S. (1993). Reversely Magnetized Flows, Rajahmundry, Andhra Pradesh. *Journal of the Geological Society of India*, *41*(1), 71–72. Retrieved from http://www.geosocindia.org/index.php/jgsi/article/view/67197

Tauxe, L., Shaar, R., Jonestrask, L., Swanson-Hysell, N. L., Minnett, R., Koppers, A. A. P., et al. (2016). PmagPy: Software package for paleomagnetic data analysis and a bridge to the Magnetics Information Consortium (MagIC) Database. *Geochemistry, Geophysics, Geosystems*, *17*(6), 2450–2463. https://doi.org/10.1002/2016GC006307

Towles, N., Olson, P., & Gnanadesikan, A. (2015). Scaling laws for perturbations in the ocean–atmosphere system following large CO2 emissions. *Climate of the Past, 11*(7), 991–1007. https://doi.org/10.5194/cp-11-991-2015

Vandamme, D., & Courtillot, V. (1992). Paleomagnetic constraints on the structure of the Deccan traps. *Physics of the Earth and Planetary Interiors, 74*(3), 241–261. https://doi.org/10.1016/0031-9201(92)90013-L

Vanderkluysen, L., Mahoney, J. J., Hooper, P. R., Sheth, H. C., & Ray, R. (2011). The Feeder System of the Deccan Traps (India): Insights from Dike Geochemistry. *Journal of Petrology, 52*(2), 315–343. https://doi.org/10.1093/petrology/egq082

Vye-Brown, C., Self, S., & Barry, T. L. (2013). Architecture and emplacement of flood basalt flow fields: case studies from the Columbia River Basalt Group, NW USA. *Bulletin of Volcanology, 75*(3), 697. https://doi.org/10.1007/s00445-013-0697-2

Watson, G. S. (1956). A Test for Randomness of Directions. *Geophysical Supplements to the Monthly Notices of the Royal Astronomical Society, 7*(4), 160–161. https://doi.org/10.1111/j.1365-246X.1956.tb05561.x

Widdowson, M., Walsh, J. N., & Subbarao, K. V. (1997). The geochemistry of Indian bole horizons: palaeoenvironmental implications of Deccan intravolcanic palaeosurfaces. *Geological Society, London, Special Publications, 120*(1), 269 LP – 281. https://doi.org/10.1144/GSL.SP.1997.120.01.17

Zeebe, R. E. (2012). LOSCAR: Long-term Ocean-atmosphere-Sediment CArbon cycle Reservoir Model v2.0.4. *Geoscientific Model Development, 5*(1), 149–166. https://doi.org/10.5194/gmd-5-149-2012
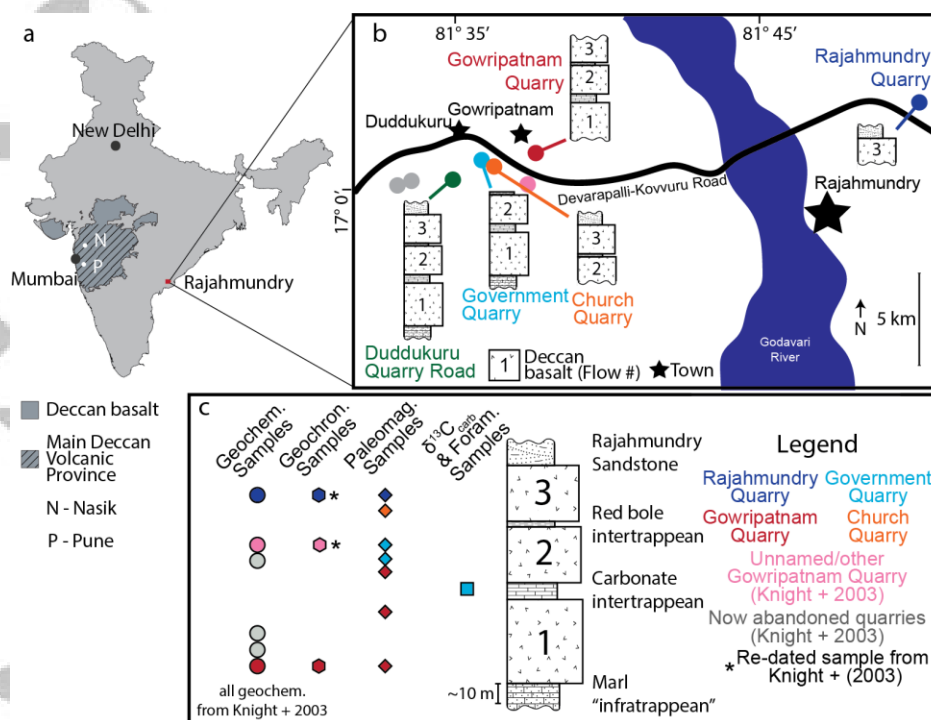
Figure 1: **a)** Map of India showing the location of the Rajahmundry Traps (RT) as well as the Main Deccan Volcanic Province (MDVP), adapted from Kale et al., 2020. MDVP eruptive centers are hypothesized to be between Mumbai, Nasik (N), and Pune (P), based on occurrence of feeder dikes (e.g., Vanderkluysen et al., 2011) **b)** Map of study localities, including which lava flows and sedimentary units are exposed at each site. **c)** Schematic stratigraphic section with samples indicated. Quarry for each sample is indicated by color. For several of the Knight et al. (2003) samples, the quarry is now flooded and abandoned.

Figure 2: a) Image showing all three flows exposed in the Gowripatnam Quarry. The finely spaced, irregular, columnar joints exhibited in Flow 1 are typical of water-cooled lavas. Note the water at the base of Flow 1 - the water table causes quarries to be flooded and consequently abandoned after they are excavated to the base of a lava flow. This leads to quarries exposing only one or two of the three flows. **b)** Image showing the Rajahmundry sandstone and Flow 3 contact from the Duddukuru Quarry Road section on the western side of the Godavari River.

Figure 3: a) Age spectra for each of the three RT flows. Uncertainties are at the 1σ level and only analytical uncertainty is shown. **b)** Paleomagnetic polarity diagrams for each of the three flows, also indicating the present normal field as well as Cretaceous reverse and Cretaceous normal directions. Open (closed) symbols indicate data plotting in the upper (lower) hemisphere. Note, at the time of eruption, India was in the southern hemisphere.
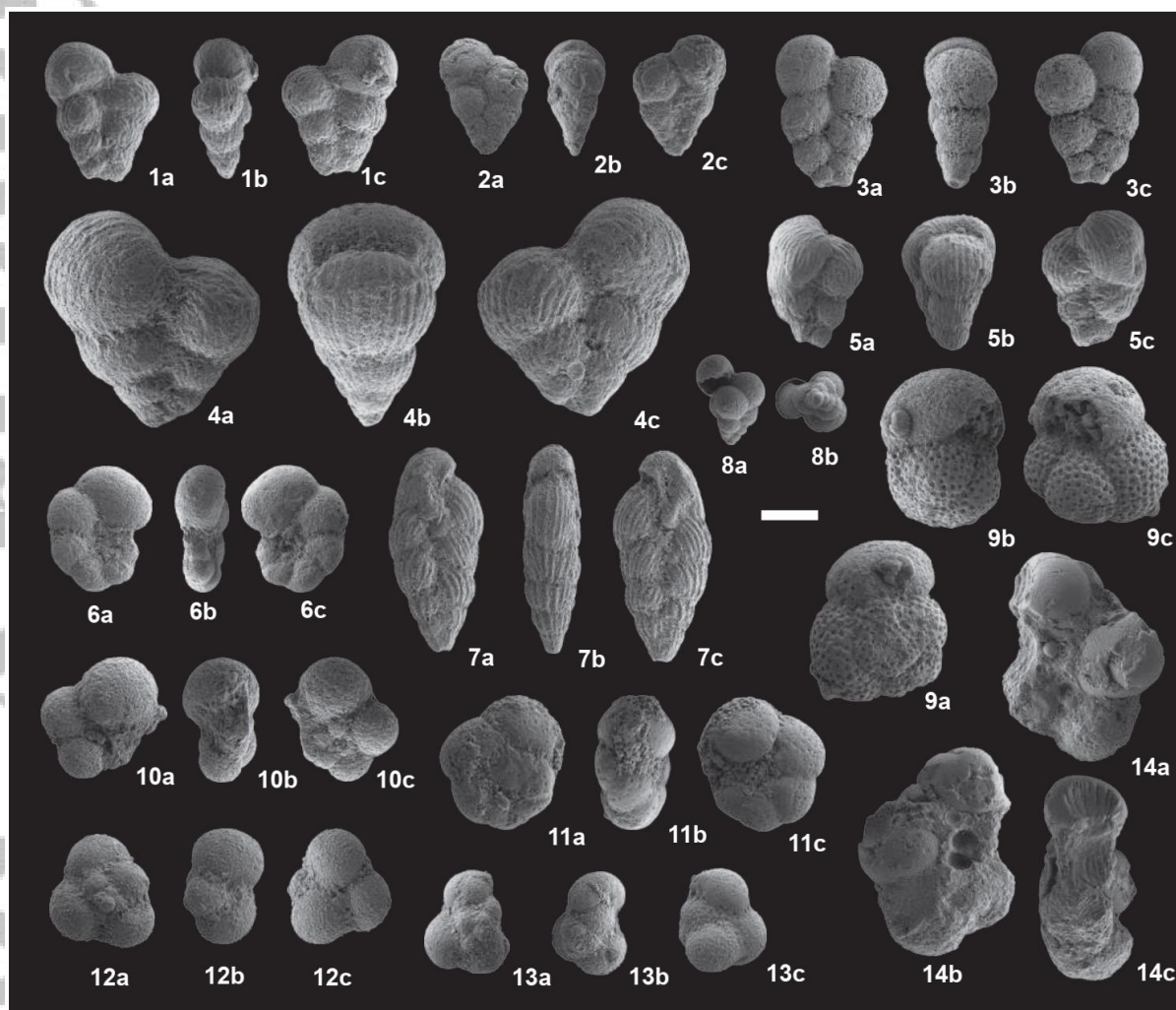
Figure 4: SEM images of the planktic foraminiferal specimens identified in the carbonate intertrappean unit of the Government Quarry section (scale bar = 100 μm). 1. *Heterohelix globulosa*, sample GQN3; 2. *Heterohelix globulosa*, sample GQN7; 3. *Heterohelix globulosa*, sample GQN10; 4. *Heterohelix* aff. *globulosa* (transitional to *Heterohelix punctulata*), sample GQN3; 5. *Heterohelix* aff. *globulosa* (transitional to *Heterohelix punctulata*), sample GQN9; 6. *Globigerinelloides rosebudensis*, sample GQN3; 7. *Pseudoguembelina costulata*, sample GQN4; 8. *Guembelitria cretacea*, sample GQN12; 9. *Eoglobigerina trivialis* (with inflated chambers) or *Subbotina triloculinoides* (with the last broken underdeveloped chamber), sample GQN10; 10. *Parasubbotina varianta*, sample GQN13; 11. *Praemurica inconstans*, sample GQN3; 12. *Globoconusa* aff. *daubjergensis*, sample GQN3; 13. *Globoconusa daubjergensis*, sample GQN10; 14. *Parasubbotina pseudobulloides* (internal mold), sample GQN11.
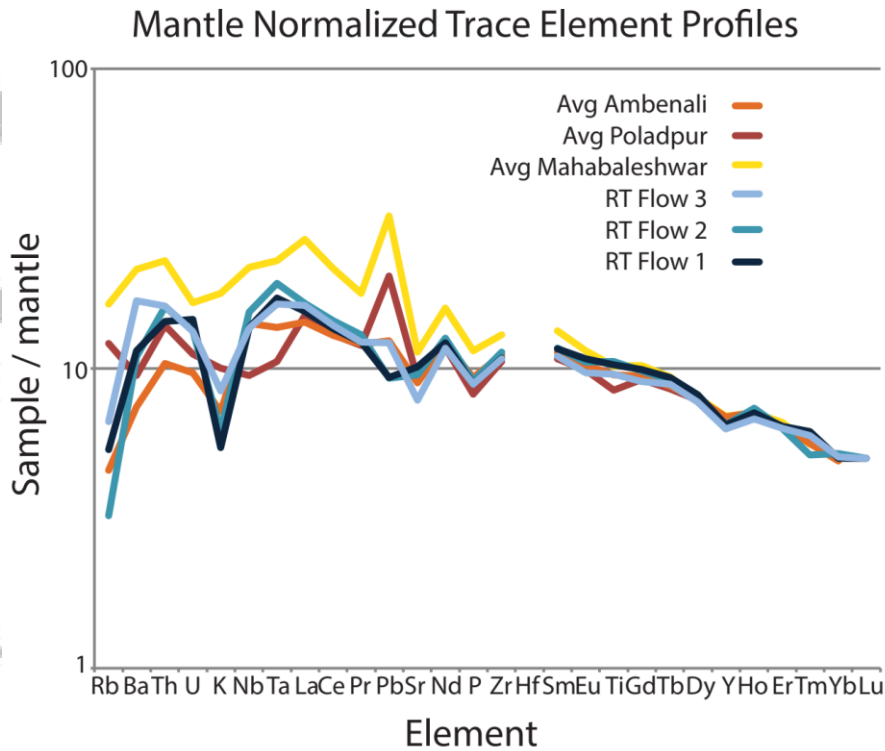
Figure 5: Mantle-normalized trace element profiles for each of the three RT flows (geochemical data from Knight et al., 2003) compared with current reference average compositions for the three Deccan formations closest in age to the RT flows: the Ambenali, Mahabaleshwar, and Poladpur Formations (Vanderkluysen et al., 2011). Mantle values are from McDonough and Sun (1994), with a Lu=5 normalization. Note the upper Mahabaleshwar Fm. is more like Ambenali than like average Mahabaleshwar. The upper Mahabaleshwar is not plotted, as a full suite of trace element data is not available.
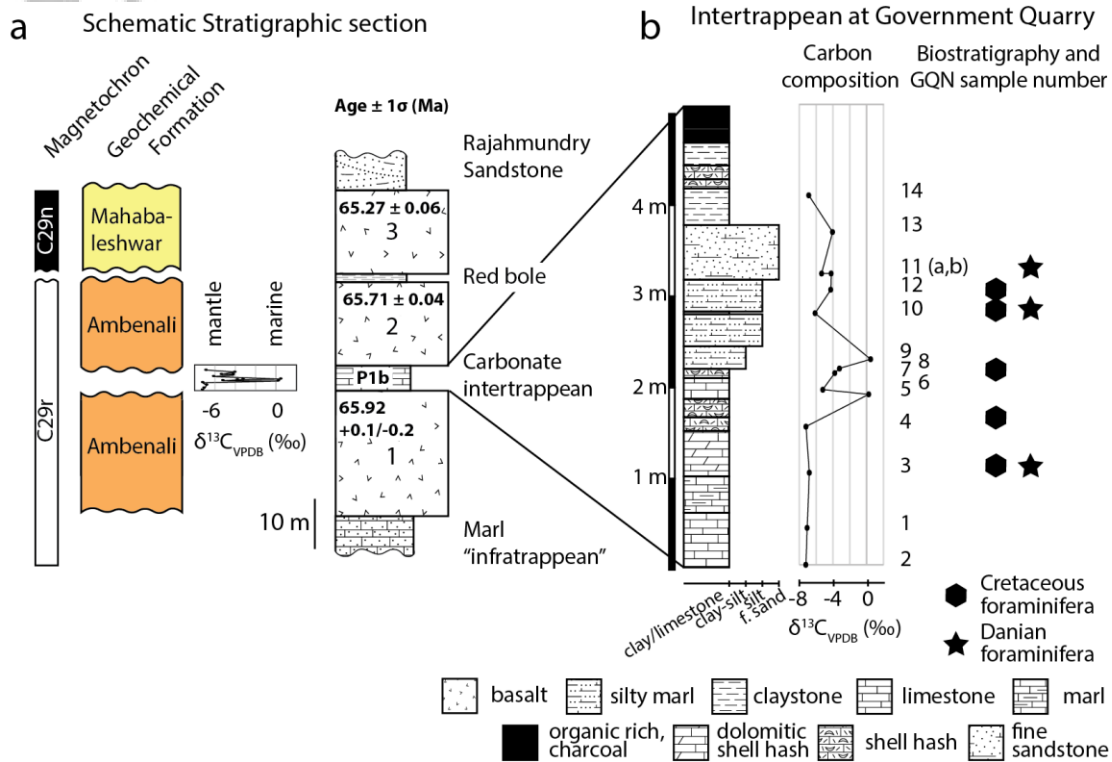
Figure 6: a) Composite stratigraphic section, showing the date, magnetic polarity, biostratigraphy, and geochemical formation for each RT flow. The age shown is the ^{40}Ar/^{39}Ar date, accounting for age constraints from magetostratigraphy and geochemistry (Text S2) **b)** Stratigraphic section of the carbonate intertrappean from the Government Quarry site, with expanded $\delta^{13}C_{carb}$ and biostratigraphy, including GQN sample numbers.
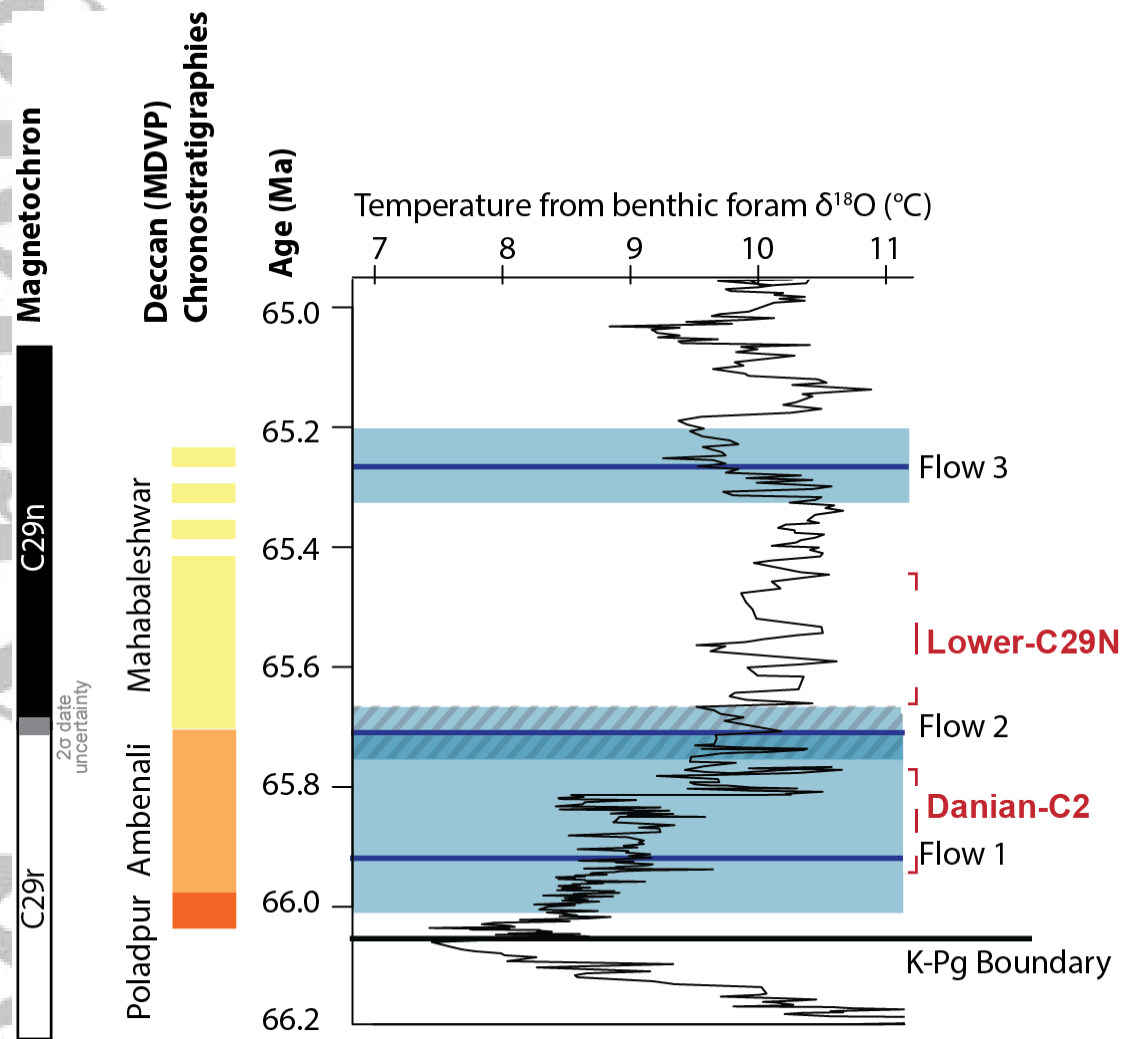
Figure 7: The age (with 1σ uncertainty shaded) of each RT flow plotted with deep ocean temperature from Barnet et al. (2019), as well as magnetostratigraphy and Deccan chronostratigraphy. The approximate age range of the Danian-C2 and Lower-C29n hyperthermals based on constraints from Barnet et al., (2019), Coccioni et al., (2010), and Sinnesael et al., (2019). Magnetostratigraphy is from Sprain et al., (2018), and the timescale for the temperature record is adjusted so the C29r/C29n boundary is isochronous through all data presented (Text S3). Deccan chronostratigraphy is from Sprain et al., (2019), combined with magnetostratigraphic constraints (Text S2). Top of the solid Mahabaleshwar bar is placed at the youngest date for the Mahabaleshwar Fm (Sprain et al., 2019), although the top of the formation remains undated.
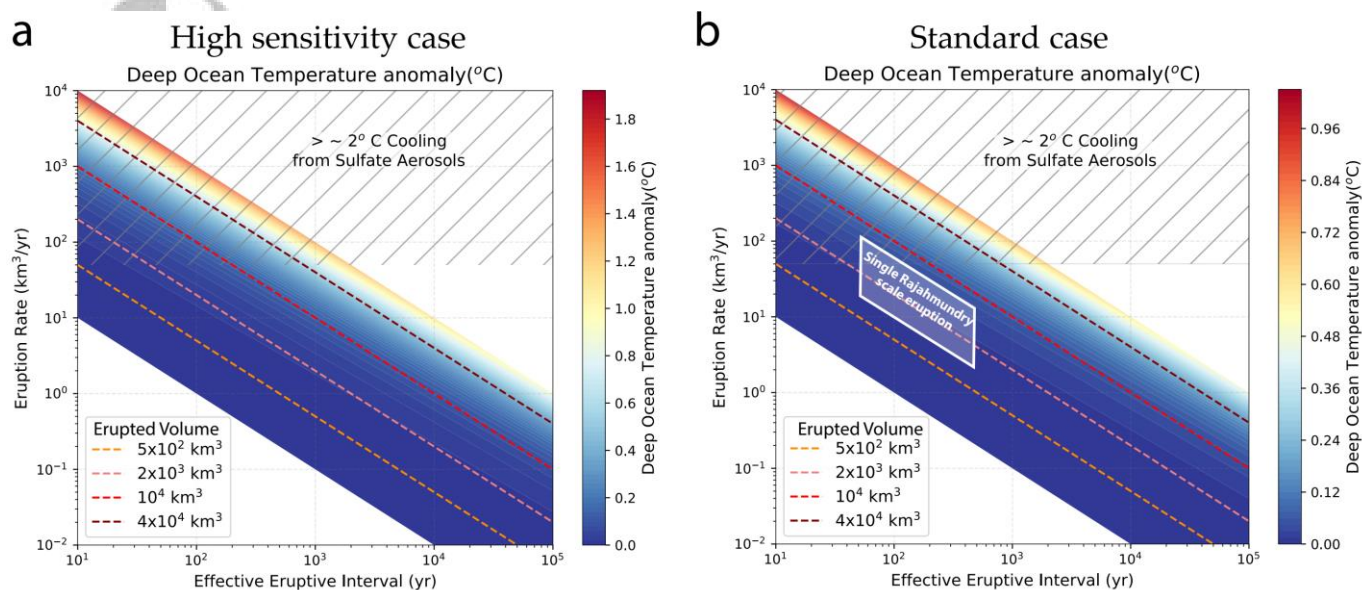
Figure 8: The peak warming observed in the deep ocean for varying volcanogenic CO2 emission rates and durations. The temperatures were calculated using emissions to temperature scaling from Towles et al., (2015) for the LOSCAR carbon cycle model (Zeebe, 2012). We assume volcanic emissions of 14 Tg CO_2 per km^3 basalt (equivalent to 0.5% CO_2 by weight, Self et al., 2006). The eruption rates for which sulfate aerosol driven cooling is expected to exceed 2°C is from Schmidt et al. (2016). In **a)** we utilize the most sensitive initial conditions: a low initial pCO2 concentration of 300 ppm, and a high equilibrium climate sensitivity of 4°C per CO_2 doubling. In **b)**, we use reasonable estimates for the early Paleocene as most likely conditions: an initial pCO_2 of 450 ppm and an equilibrium climate sensitivity of 3 C per CO_2 doubling. The best estimates for an individual Rajahmundry-scale large eruption (~1000-6000 km^3 in 50-500 years) are indicated with a white parallelogram.